

# **Erosion Potential of a Burn Site in the Mojave-Great Basin Transition Zone: Interim Summary of One Year of Measurements**

prepared by

V. Etyemezian, D. Shafer, J. Miller, I. Kavouras, S. Campbell,  
D. DuBois, J. King, G. Nikolich, and S. Zitzer

submitted to

Nevada Site Office  
National Nuclear Security Administration  
U.S. Department of Energy  
Las Vegas, Nevada

March 2010

**Publication No. 45233**

Reference herein to any specific commercial product, process, or service by trade name, trademark, manufacturer, or otherwise, does not necessarily constitute or imply its endorsement, recommendation, or favoring by the United States Government or any agency thereof or its contractors or subcontractors.

Available for sale to the public from:

U.S. Department of Commerce  
National Technical Information Service  
5301 Shawnee Road  
Alexandria, VA 22312  
Phone: 800.553.6847  
Fax: 703.605.6900  
Email: [orders@ntis.gov](mailto:orders@ntis.gov)  
Online ordering: <http://www.osti.gov/ordering.htm>

Available electronically at <http://www.osti.gov/bridge>

Available for a processing fee to the U.S. Department of Energy and its contractors, in paper, from:

U.S. Department of Energy  
Office of Scientific and Technical Information  
P.O. Box 62  
Oak Ridge, TN 37831-0062  
Phone: 865.576.8401  
Fax: 865.576.5728  
Email: [reports@adonis.osti.gov](mailto:reports@adonis.osti.gov)

# **Erosion Potential of a Burn Site in the Mojave-Great Basin Transition Zone: Interim Summary of One Year of Measurements**

prepared by

V. Etyemezian<sup>1</sup>, D. Shafer, J. Miller, I. Kavouras<sup>1</sup>, S. Campbell, D. DuBois<sup>1</sup>, J.  
King<sup>1</sup>,  
G. Nikolich<sup>1</sup>, and S. Zitzer<sup>3</sup>

<sup>1</sup>Division of Atmospheric Sciences, <sup>2</sup>Division of Hydrologic Sciences,  
<sup>3</sup>Division of Earth and Ecosystem Sciences  
Desert Research Institute  
Nevada System of Higher Education

Publication No. 45233

submitted to

Nevada Site Office  
National Nuclear Security Administration  
U.S. Department of Energy  
Las Vegas, Nevada

March 2010

---

The work upon which this report is based was supported by the U.S. Department of Energy under Contract # DE-AC52-06NA26383. Approved for public release; further dissemination unlimited.

**THIS PAGE LEFT INTENTIONALLY BLANK**

## ABSTRACT

A historic return interval of 100 years for large fires in deserts in the Southwest U.S. is being replaced by one where fires may reoccur as frequently as every 20 to 30 years. This increase in fires has implications for management of Soil Sub-Project Corrective Action Units (CAUs) for which the Department of Energy, National Nuclear Security Administration Nevada Site office (NNSA/NSO) has responsibility. A series of studies has been initiated at uncontaminated analog sites to better understand the possible impacts of erosion and transport by wind and water should contaminated soil sites burn over to understand technical and perceived risk they might pose to site workers and public receptors in communities around the NTS, TTR, and NTTR; and to develop recommendations for stabilization and restoration after a fire. The first of these studies was undertaken at the Jacob fire, a lightning-caused fire approximately 12 kilometers north of Hiko, Nevada, that burned approximately 200 ha between August 6-8, 2008, and is representative of a transition zone on the NTS between the Mojave and Great Basin Deserts, where the largest number of Soil Sub-Project CAUs/CASs are located. The area that burned was primarily a *Coleogyne ramosissima* (blackbrush) and *Ephedra nevadensis* (Mormon tea) community, an abundant shrub assemblage in the transition zone on the NTS. This report summarizes the first year of measurements after the fire.

At the time of this report, four measurement efforts at the Jacob fire site had been completed: 1 month after the burn (MAB), 3 MAB, 6 MAB, and 13 MAB. Additional measurements are planned for 18 MAB, 24 MAB, and 36 MAB in order to capture longer-term trends in how the soil erodibility changes after a fire event. Runoff and water erosion of soils was quantified through a series of rainfall/runoff simulation tests, whereby controlled amounts of water were delivered to the soil surface in a set amount of time. Measurements were completed on native desert that was not subjected to fire that served as a control area; as well as areas along ridges and in channels or washes that were burned. In each case, tests were completed on plant mounds and in between plant mounds (interspaces). Wind erosion quantification was conducted with a similar philosophy, with measurements conducted on native desert, burned ridges, and burned wash areas. For the latter two cases, plant mounds and interspaces were separately tested. A portable wind tunnel-style instrument (PI-SWERL) was used to estimate emissions of suspendable particles (PM<sub>10</sub>, corresponding to particles with aerodynamic diameter smaller than 10 microns) at different wind speeds. Context for these measurements was provided through a meteorological tower that was installed at the Jacob site to obtain local, relevant environmental parameters. Filter samples, collected from the exhaust of the PI-SWERL during measurements, were analyzed for chemical composition. In addition, vegetation transects were conducted in the control area native vegetation as well as in the area that burned.

After the first year of measurements, several preliminary trends were observed, although we note that the measurements also indicate that there are substantial seasonal influences on almost all parameters measured and firm conclusions regarding long-term trends are not appropriate at this time. PI-SWERL measurements indicated the potential for PM<sub>10</sub> windblown dust emissions was higher on areas that were burned compared to areas that were not. Among the burned areas, charred plant mounds located in washes were the most

emissive, and interspace areas between plant mounds along burned ridges were least emissive. Comparing measurements at 1 and 13 MAB — when environmental conditions were likely the most similar — there remained substantial differences in emissions between burned and unburned areas, indicating that the effects of the fire had not been dampened by the passage of one year. Preliminary analysis of PM<sub>10</sub> filter samples collected from the PI-SWERL exhaust indicated that the fraction of PM<sub>10</sub> attributable to carbon one month after the fire was higher on burned areas than the surrounding native desert.

Rainfall simulation measurements suggested that fire may have a complex effect on infiltration and runoff. Some burned surfaces initially (1 MAB) exhibited high runoff potential followed by lower runoff potential (at 3 and 6 MAB), with a return to higher potential at 13 MAB. One hypothesis for this trend is that post-fire runoff may have been initially most influenced by hydrophobicity that reduced soil infiltration and increased runoff. In later months, the hydrophobic effect was reduced, and the soil aggregates that were loosened by the fire were comparatively easier for water to infiltrate into. As more time passed, the soil structure collapsed, reducing pore spaces, increasing bulk density and reducing infiltration capacity.

Longer-term measurements as well as measurements at other fire sites will assist in developing a more comprehensive picture of soil behavior after a fire event and testing hypotheses related to mechanisms of erosion modification by fire.

## **ACKNOWLEDGMENTS**

Thanks are extended to Karen Prentice of the U.S. Bureau of Land Management Ely Field Office who provided National Environmental Policy Act coverage for the research being conducted at the site, as well as providing insight on other fires that have occurred in recent years in this part of Nevada. Kent Ostler and Ashley Burns of National Security Technologies provided data on the distribution of the blackbrush and Mormon tea shrub assemblage on the NTS. The work was carried out under DRI's Technical Research, Engineering, and Development Services Contract (No. DE-AC52-06NA26383) for the U.S. Department of Energy, National Nuclear Security Administration Nevada Site Office.

**THIS PAGE LEFT INTENTIONALLY BLANK**

## CONTENTS

Abstract.....	iii
Acknowledgments .....	v
List of Figures .....	viii
List of Tables.....	viii
Introduction .....	1
Implications for Soil Sub-Project Sites.....	1
Ecological Regions of the Nevada Test Site and the Jacob Fire .....	2
The Jacob Fire.....	3
Methods .....	5
Meteorological Instruments .....	6
PI-SWERL Measurements.....	7
Filter Samples and Analysis .....	8
Runoff Measurements.....	9
Results.....	11
Meteorology.....	11
PI-SWERL Measurements.....	15
Filter Samples and Analysis .....	19
Runoff Measurements.....	21
Moisture Content .....	23
Collected Runoff Volumes and Particle Sizes.....	23
Preliminary Conclusions .....	30
References .....	31
Appendix: supplemental data.....	33

## LIST OF FIGURES

1. Distribution of the / <i>Coleogyne remosissima</i> /Torr. and / <i>Ephedra nevadensis</i> / shrub alliance on the Nevada Test Site (NTS). .....	3
2. Jacob fire location and extent. ....	4
3. Photograph of portable rainfall simulator.....	5
4. Photograph of Jacob burn site .....	6
5. Cumulative emissions ( $\text{g}/\text{m}^2$ ) calculated at different points during the PI-SWERL measurement cycle. ....	8
6. Monthly temperature at Jacob site.....	12
7. Monthly relative humidity at Jacob site .....	12
8. Temperature of soil in top 1 cm at Jacob site.....	13
9. Monthly soil volumetric water content and total monthly precipitation (cm) at Jacob site. ....	13
10. Monthly average and maximum wind speeds at Jacob site.....	14
11. Wind rose from Jacob's fire site (10/08–9/09).....	14
12. PI-SWERL results at 1 MAB .....	15
13. PI-SWERL results at 3 MAB .....	16
14. PI-SWERL results at 6 MAB. ....	16
15. PI-SWERL results at 13 MAB .....	17
16. $\text{PM}_{10}$ emissions at the end of the 3000 RPM Step (24 mph sustained) at 1, 3, 6, and 13 MAB.....	18
17. Abundance of elements associated with soil minerals. ....	19
18. Abundances of carbon compounds.....	19
19. Abundances of water-soluble species.....	20
20. Abundances of common elements.....	20
21. Abundances of rare elements.....	21
22. Runoff hydrographs from the various test plots, over time, at Jacob Fire site. A: Burned Ridge, Plant Mound. B: Burned Ridge, Interspace .....	25
23. Runoff hydrographs from the various test plots, over time, at Jacob Fire site. C: Burned Channel, Plant Mound. D: Burned Channel, Interspace.....	26
24. Runoff hydrographs from the various test plots, over time, at Jacob Fire site. E: Unburned, Plant Mound. F: Unburned, Interspace.....	27
25. Comparison of particle size distributions at the burned channel plant mound and burned ridge interspace test plots between September 2008 and November 2008 sampling events. ....	28
26. Comparison of particle size distributions at the burned and unburned interspace test plots between September 2008 and November 2008 sampling events. ....	29

## LIST OF TABLES

1. Curve numbers for the first measurements made at the Jacob Site.....	21
2. Moisture content results of in-situ (initial) vs. post-rain (final) soils.....	24

## INTRODUCTION

Since the mid-1980s, the frequency and size of fires have increased throughout the western U.S., correlating with an increase in average spring and summer temperatures, which may be contributing to earlier loss of soil moisture and longer periods of dry plant biomass (particularly from annual plants) on the surface (Westerling *et al.*, 2006). Regionally, average spring and summer temperatures for the period 1987 to 2003 were 0.87 °C higher than the period 1970 to 1986. Contributing factors in the Great Basin and elsewhere in the Southwest U.S., including Nevada, are drought conditions across large areas of the region since 1999; the spread of invasive annual grasses, most significantly cheatgrass (*Bromus tectorum*) and red brome (*Bromus rubens*); and particularly during the 20<sup>th</sup> century, accumulated fuel loads due to wildfire suppression (Savage and Swetnam, 1990; Neary *et al.*, 1999; Westerling and Swetnam, 2003; Westerling *et al.*, 2006).

A historic return interval of 100 years for large fires in deserts in the Southwest U.S. is being replaced by one where fires may reoccur as frequently as every 20 to 30 years (Brooks, 2006). A measure of the magnitude of changing fire regimes is that between 1998 and 2008, an average of nearly 850,000 hectares (ha) per year burned in the Great Basin, including more than 1 million ha in 2007 (Chambers *et al.*, 2008). Most indicative of the changing fire regime in the region, were a series of 11 fires that burned approximately 300,000 ha in southern Nevada and Utah, including 206,000 ha in Nevada alone between June 22 and July 10, 2005. The “Southern Nevada Complex Fire” were lightning-caused, but followed a period of above average precipitation in the fall of 2004 and winter of 2004 and 2005 that caused a significant buildup of invasive grasses and annuals in the southern Great Basin and Mojave Desert which helped to carry the fires (National Interagency Coordination Center, 2006). While certainly not of the same scale in area, in early June 2005, the so-called “Air Force Fire,” also sparked by lightning, burned approximately 8,000 ha of the NTTR and an additional 2,400 ha on the west side of the NTS (NNSA, 2005). During the course of the fire, there was concern that some contaminated soil sites on Buckboard Mesa and Dome Mountain on the NTS could burn over, although the fire was contained before this happened.

### Implications for Soil Sub-Project Sites

The increase in fires in arid and semi-arid parts of Nevada and elsewhere in the Southwest U.S. has implications for post-closure management or long-term stewardship for Soil Sub-Project Corrective Action Units (CAUs) for which the Department of Energy, Nevada Nuclear Security Administration Nevada Site office (NNSA/NSO) has responsibility for regulatory closure. For many CAUs and Corrective Action Sites (CASs) where closure-in-place alternatives are now being implemented or considered, there is a greater chance that they could burn over at some point while they still pose a risk, especially considering the long half-life of some of the radionuclide contaminants of concern (COCs) (Shafer *et al.*, 2007; Shafer and Gomes, 2009).

Although the Nevada Applied Ecology Group (NAEG), primarily in the 1970s, examined a variety of disturbance mechanisms at Soil Sub-Project CAUs where isotopes of Plutonium were among the most significant (COCs), fires were not considered because at that time they were comparatively infrequent and small in size (Bruce Church and Lynn Anspaugh, personal communication, 2007). The majority of NAEG studies were carried out before the spread of cheatgrass (*B. tectorum*) and red brome (*B. rubens*) across the area

encompassing the NTS, the Tonopah Test Range (TTR), and the Nevada Test and Training Range (NTTR). Both grasses were introduced to the region as part of Euro-American settlement and cattle grazing in the nineteenth century (Knapp, 1996). Although both plants were found locally on disturbed sites as early as the 1960s on the NTS, both species spread across the region during a period of above-average precipitation in the 1980s (Hunter, 1991; Rickard and Beatley, 1965). Today, these grasses can rapidly invade disturbed areas and in many plant communities they have colonized interspaces between shrubs, increasing the total fuel load, but also allowing fires to move more easily between shrubs (Knapp, 1996). Besides increasing the chance of a fire occurring and the likelihood that it will burn larger areas than historic fires, Hansen and Ostler (2004) have documented that invasive plants are quick to colonize areas that have burned on the NTS, increasing the chance that subsequent fires will occur.

To better understand the implications and risks should Soil Sub-Project CAUs/CASs burn over, a series of studies has been initiated at uncontaminated analog sites to better understand the possible impacts of erosion and transport by wind and water, the risks and perceived risk they might pose to site workers and public receptors in communities around the NTS, TTR, and NTTR; and to develop recommendations for stabilization and restoration of contaminated sites should they burn over. The first of these studies was undertaken at the Jacob fire, representative of a transition zone on the NTS between the Mojave and Great Basin Deserts (Ostler *et al.*, 2000) where the largest number of Soil Sub-Project CAUs/CASs are located. This report focuses on the first year after the fire.

### **Ecological Regions of the Nevada Test Site and the Jacob Fire**

Ostler *et al.* (2000) and earlier workers (mostly prominently, Beatley, 1976) identified three ecological regions on the Nevada Test Site (NTS): the northern Mojave Desert, the Great Basin, and the Mojave/Great Basin Transition Zone (see Figure 1). The Transition Zone Ecoregion represents 36.6 percent of the total land area of the NTS (Ostler *et al.*, 2000). Within the Transition Zone, the dominant shrubland alliance is the blackbrush (*Coleogyne remosissima* Torr.)/Mormon Tea (*Ephedra nevadensis*), which in some cases consists of nearly pure stands of blackbrush. Although it occurs elsewhere in the southern part of the NTS (21.6 percent of the NTS in total), it is especially dominant on mid to upper piedmont slopes surrounding Yucca Flat as well as Mid Valley and Topopah Valley. Yucca Flat areas where it occurs have frequently been disturbed by nuclear testing, including areas that are now part of Soils Sub-Project CASs of Northern Yucca Flat, portions of Plutonium Valley, as well as the west side of the basin. On the NTS, it occurs primarily in areas of undisturbed shallow soils on quaternary alluvial and colluvial fans with moderate desert pavement development. Soils are generally loams to sand loams. Although elsewhere in Nevada and adjoining states the blackbrush/Mormon tea shrubland develops most frequently on Tertiary volcanic tuffs, on the NTS it also forms on limestone-dominated substrates.

Blackbrush has traditionally been considered a highly flammable species; in recent years, its susceptibility to fires has been increased by the presence of invasive annual grasses at many sites. Recovery times for blackbrush after fires vary. However, it has often taken 50, and sometimes as many as 100 years for it to recover (Sugihara, 2006).

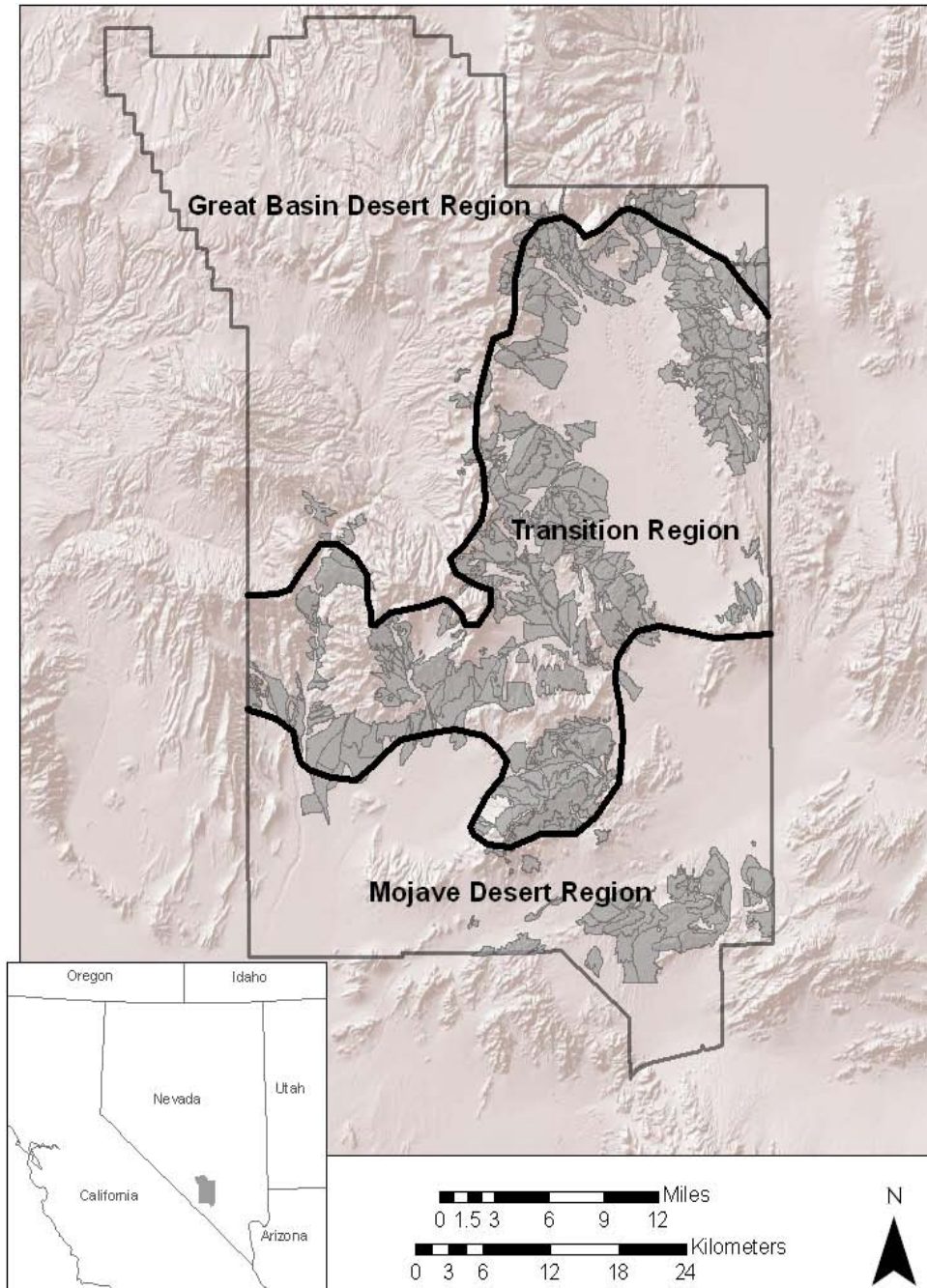


Figure 1. Distribution of the *Coleogyne remossissima* Torr. and *Ephedra nevadensis* shrub alliance on the Nevada Test Site (NTS). Although not confined exclusively to it, the shrub alliance is most indicative of the Great Basin-Mojave Desert Transition Region on the NTS. Data from Hansen and Ostler (2004)

### The Jacob Fire

The Jacob fire (37°42'17" 115°12'41"W) was a lightning-caused fire approximately 12 kilometers north of Hiko, Nevada, that burned approximately 200 ha between August 6-8, 2008 (Figure 2). The area is managed by the U.S. Bureau of Land Management

(BLM). Among the reasons the Jacob fire was selected as an analog study site for fires in the Mojave-Great Basin Transition Zone of the NTS were the following:

- The area burned was dominated by blackbrush and Mormon tea.
- The elevation range of the fire (1200 to 1500 m) is similar to those at margins of the Yucca Flat on the NTS.
- The alluvial/colluvial material on which the fire occurred is dominated by clasts derived from volcanic tuffs (Taylor and Bartley, 2002).
- Similarity in annual precipitation. Based on National Oceanic and Atmospheric Administration (NOAA) weather stations, yearly precipitation at Station BJJ (elevation 1,241 m) on the north end of Yucca Flat on NTS averaged 163 millimeters (mm) based on records between 1960 to 2006 record. ([http://www.sord.nv.doe.gov/home\\_climate\\_MEDA.htm](http://www.sord.nv.doe.gov/home_climate_MEDA.htm)). Although there is no long-term record available for the Jacob fire site proper, the town of Hiko averaged 170 mm annually between 1999 and 2009 (<http://www.wrcc.dri.edu/cgi-bin/cliGCCStP.pl?nv3671>), with a similar percentage (18%) occurring in the summer as at BJJ on the NTS (17%).

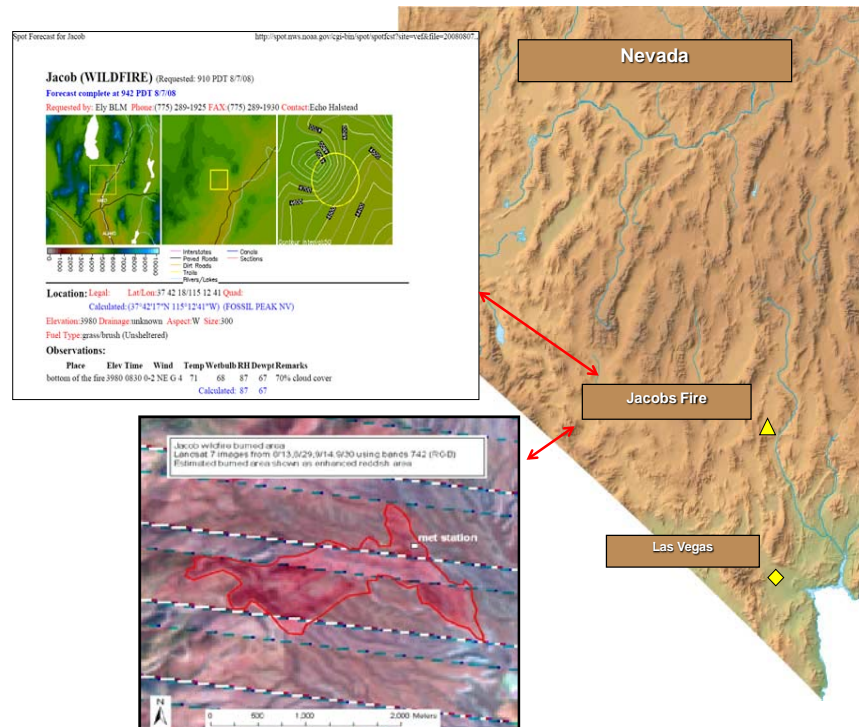


Figure 2. Jacob fire location and extent.

At the time of this report, four measurement efforts at the Jacob fire site have been completed. These occurred at 1 month after the burn (MAB), 3 MAB, 6 MAB, and 13 MAB. During all four efforts, the Portable In Situ Wind Erosion Lab (PI-SWERL) instrument was used to quantify emissions of  $PM_{10}$  at various simulated wind speeds. These measurements were conducted on areas that were affected by the burn as well as areas that were not (serves

as baseline). In conjunction with PI-SWERL measurements, PM<sub>10</sub> particles were collected on filter media and subjected to chemical analyses. These analyses are intended to reveal differences between PM<sub>10</sub> emitted from burned areas and unburned areas as well as changes in PM<sub>10</sub> chemical composition over time. Estimates of runoff and soil erosion potential, obtained with a portable rainfall simulator (PRS) (Figure 3) were also collected on different types of surfaces on four occasions over the period from September 2008 through November 2009.



Figure 3. Photograph of portable rainfall simulator.

## METHODS

The basic approach for characterizing the effects of fire on the chemistry of wind-suspendable particles and the potential for wind and water erosion has been to conduct measurements on the area that was burned by the wild fire (Figure 4) and parallel measurements on areas that are part of the same landscape geomorphically and ecologically that were not affected by the wildfire. These latter measurements on “native desert” serve to provide a baseline for comparing how fire may have affected the landscape at the Jacob site. The measurement schedule was designed with the presumption that changes in soil properties after the fire would probably be most pronounced immediately after the fire, and become less dramatic over time. Thus, on-site measurements were conducted at 1 month after the burn (MAB), 3 MAB, 6 MAB, and 13 MAB. Additional measurements are planned at 18 MAB, 24 MAB, and 36 MAB in order to capture longer-term trends in how the soil erodibility changes after a fire event.

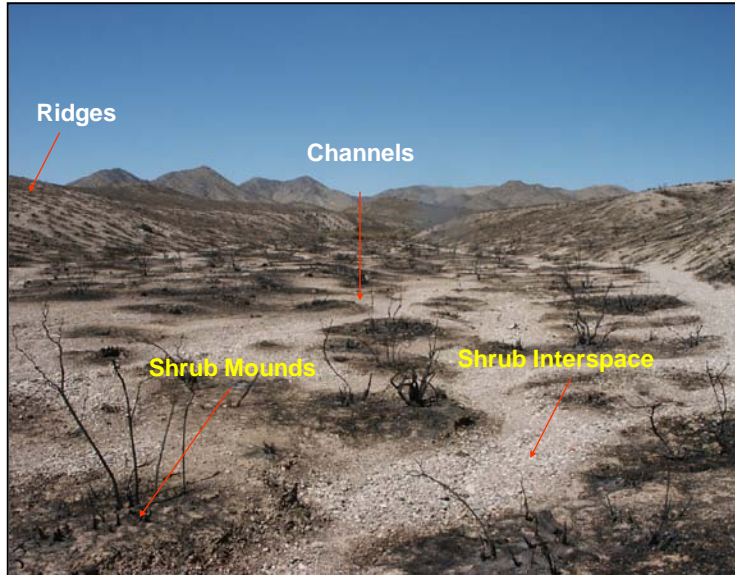


Figure 4. Photograph of Jacob burn site

Runoff and water erosion of soils was quantified through a series of rainfall/runoff simulation tests, whereby controlled amounts of water are delivered to the soil surfaces with a device that simulates rainfall. Measurements were completed on native desert that was not subjected to fire, areas along ridges that were burned during the fire, and areas along channels or washes that were burned. In each of these cases, test were completed on plant mounds and in between plant mounds (interspace) because plant mounds and interspace regions do have different hydrologic characteristics on the NTS and elsewhere in the Southwest U.S. (e.g., Shafer *et al.*, 2007).

Wind erosion quantification was conducted with a similar philosophy, with measurements conducted on native desert, burned ridges, and burned wash areas. For the latter two cases, plant mounds and interspace regions were separately tested. A PI-SWERL was used to estimate emissions of suspendable particles ( $PM_{10}$ , corresponding to particles with aerodynamic diameter smaller than 10 microns) at different wind speeds. Context for these measurements was provided through a meteorological tower that was installed at the Jacob site to obtain local wind speed, wind direction, and other relevant environmental parameters such as soil moisture.

Filter samples, collected from the exhaust of the PI-SWERL during measurements, were analyzed for chemical composition. Due to concerns about minimum loading, filter samples represent aggregated samples of dust emitted from both plant mound and interspace areas, although separate sets of filters were obtained for native desert, burned wash, and burned interspace areas.

### **Meteorological Instruments**

A meteorological station was installed at the Jacob burn site in October 2008 (3 MAB) to monitor wind and other environmental parameters. The station consisted of a 3-meter-high post, mounted on a tripod, and anchored to the ground for stability. The station

was instrumented for measuring ambient air temperature and relative humidity (HMP 50), wind speed and direction (CS 3002), precipitation (TE 525), soil temperature (CS 107), and soil volumetric water content (CS 616) near the surface. All instruments are scanned once every 5 seconds and data were processed and stored on a data logger (Campbell Scientific, CR 1000) in intervals of ten minutes. The datalogger has sufficient on-board memory to accommodate three months of continuous operation and the entire station was powered by a solar panel and a battery to provide power overnight.

### PI-SWERL Measurements

The PI-SWERL was operated at five types of locations at the Jacob fire site: Locations that were not affected by the wildfire (“native desert”, 8 replicate measurements per site visit), burned areas in washes with visible black charring (generally near where a plant used to be, “burned – plant mound – wash”, 4 replicates per site visit), burned areas in washes without visible charring (generally in the plant inter-space, “burned – interspace – wash”, 4 replicates per site visit), charred burned areas on ridges (“burned – plant mound – ridge”, 4 replicates per site visit), and burned areas on ridges without charring (“burned – interspace – ridge”, 4 replicates per site visit). Filter samples of suspended particles were also collected for each type of location, except that measurements from charred and not charred locations were conducted on the same set of filters (see filter sampling methods below).

For all measurements, a hybrid ramp/step measurement cycle was used. The cycle consisted of 1) a 60 second clean air flush, 2) sharp acceleration to 500 revolutions per minute (RPM), 3) 60 second linear ramp to 2000 RPM, 4) maintain 2000 RPM for 60 seconds, 5) 60 second ramp to 3000 RPM, 6) maintain 3000 RPM for 90 seconds, 7) 60 second ramp to 4000 RPM, 8) maintain 4000 RPM for 90 seconds, and 9) turn off motor and clean air flush for 60 seconds.

Each value of RPM corresponds to a friction velocity,  $u_*$ , that is a measure of the amount of wind shear applied to a soil surface. Friction velocity can be related to surface wind speed (measured at a height above ground level) and the surface roughness with the Prandtl Equation:

$$\frac{u_{ref}}{u_*} = \frac{1}{\kappa} \cdot \ln\left(\frac{z_{ref}}{z_0}\right) \quad (1)$$

where  $u_{ref}$  is the wind speed measured at a reference height  $z_{ref}$  (usually 10 meters),  $\kappa$  is the von Karman constant equal to 0.41, and  $z_0$  is the aerodynamic roughness height. The roughness height determines how the wind speed translates into shear stress at the soil surface. Values of  $z_0$  vary depending on the physical roughness of a surface. Typical values are: for smooth ice 0.2 mm, for grasslands 30 mm, for urban areas 500 mm, and for flat desert terrain 5 mm.

Cumulative emissions ( $\text{g/m}^2$ ) were calculated at several different points during the PI-SWERL test cycle (Figure 5). This parameter answers the questions “How much  $\text{PM}_{10}$  is initially emitted at specific wind speeds and how much  $\text{PM}_{10}$  is available for emissions at prolonged exposure to specific wind speeds?”

Cumulative emissions were calculated at the end of the ramp to 2000 RPM, at the end of the 2000 RPM Step, at the end of the ramp to 3000 RPM, at the end of the 3000 RPM step,

at the end of the ramp to 4000 RPM, and at the end of the 4000 RPM step. Values of cumulative emissions at each of these points were averaged over replicate measurements for the same types of location. For example, for all PI-SWERL measurements completed on burned wash areas with visible black charring, the cumulative emissions at the end of the ramp to 2000 RPM were averaged together. For reference, assuming that the roughness height for a desert surface is 5 mm, 2000 RPM translates roughly to a sustained wind speed of 17 mph, 3000 RPM translates to 23 mph, and 4000 RPM translates to 29 mph.

### Filter Samples and Analysis

Filter samples were collected at the exhaust port of the PI-SWERL chamber. Filter sampling apparatus included size selective inlets (SSI) to collect only particles in the PM<sub>10</sub> size range, flow control valve to ensure that flow rates (5 liters per minute) were appropriate for the correct operation of the SSI, a filter holder, and suction source to maintain flow through the filters. Particles were sampled onto two types of filters in each case, Teflon and quartz fiber. Teflon filters were subjected to gravimetric analysis (for particle mass) and X-ray fluorescence (XRF) spectroscopy to quantify the elemental composition. A portion of the quartz fiber filter was analyzed for elemental carbon, organic carbon and carbonate using the DRI thermal/optical carbon analyzer that is based on the preferential oxidation of organic

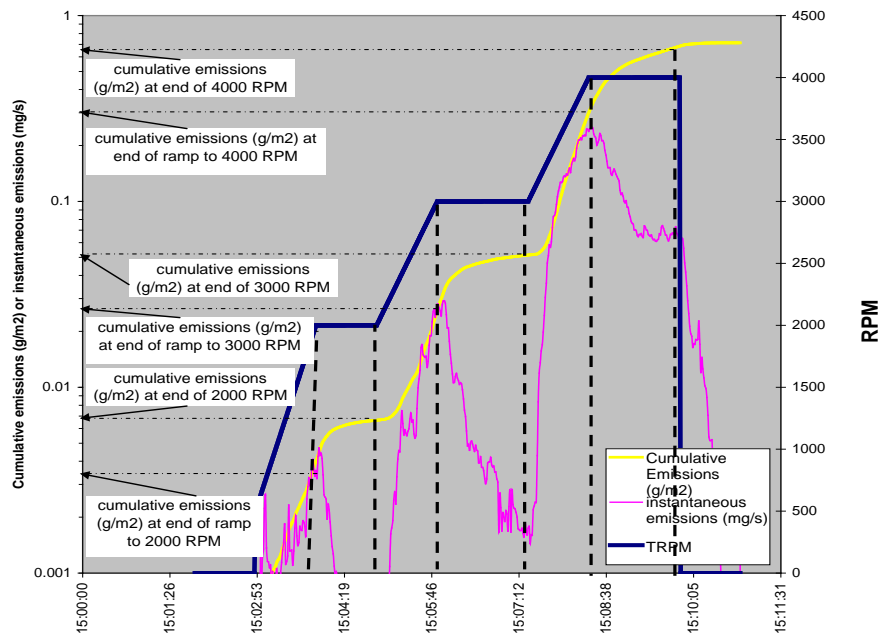


Figure 5. Cumulative emissions ( $\text{g}/\text{m}^2$ ) calculated at different points during the PI-SWERL measurement cycle.

carbon (OC) and elemental carbon (EC) compounds at different temperatures. Major water-soluble anions (chloride, nitrate and sulfate) and cations (sodium, magnesium, ammonium, calcium and potassium) were analyzed with a DIONEX500 ion chromatography system.

In order to ensure adequate filter loading, one set of filters (one Teflon, one quartz) was used for each of the three types of soil surfaces measured (Native Desert, Burned Ridge,

Burned wash). Therefore, each set of filters represents a composite of multiple (generally eight) PI-SWERL measurements.

Chemical characteristics of PM<sub>10</sub> samples are reported in terms of emission profiles or normalized abundances, where the mass of a compound or element on the filter sample is divided by the total mass of PM<sub>10</sub> particles. This type of normalized concentration is more appropriate for examining differences in chemical composition between samples than the absolute mass of a constituent.

### **Runoff Measurements**

Standard statistical methods (WRC, 1981) to determine flood discharges are not applicable to a majority of watersheds in the Southwest U.S. because most watersheds in this region are ungaged and do not have stream discharge data. Watersheds that do have discharge data usually have short periods of record with many years of no flow. Therefore, rainfall-runoff models, such as HEC-1 and HEC-HMS developed by US Army Corps of Engineers' Hydrologic Engineering Center (HEC), are used to estimate flood discharges. Methods described in local drainage design guidance manuals, such as the Clark County (Nevada) Regional Flood Control District's (CCRFC) Hydrologic Criteria and Drainage Design Manual (CCRFC, 1999) are used to estimate the input parameters required for these models in jurisdictions throughout the region.

One critical parameter for these models is the initial abstraction ( $I_a$ ) and infiltration loss of precipitation. Initial abstraction is the amount of precipitation that infiltrates into the soil prior to the occurrence of any runoff. Most rainfall-runoff models do not directly account for the  $I_a$  and infiltration losses, rather they rely on precipitation loss components that are considered to be sub-basin or overland flow area averages. The Soil Conservation Service (SCS) (now Natural Resource Conservation Service) curve number (CN) approach (USDA-SCS, 1986) is commonly used to account for precipitation losses and is recommended by the CCRFC (1999). This method for estimating rainfall excess was developed from studies of natural rainfall and runoff from small (less than 10 acres) agricultural watersheds in the mid-west and southeast United States (USDA-SCS, 1986), where the method has been shown to produce reasonable results. However, the one study of the semi-arid southwest (Hjelmfelt, 1991) did not produce satisfactory results. Also, the SCS CN approach assumes that one  $I_a$  value is appropriate for precipitation events of all return periods; however, this may not be correct.

The SCS method relates the drainage characteristics of soil groups to a CN (USDA-SCS, 1986). This relation is based on soil group classification, vegetative cover, land use type (urban, agricultural, or desert), and antecedent moisture conditions (AMC), based on the amount of rainfall in the prior five to 30 days. Curve numbers range from 100, which represents a completely impervious surface, to values less than 100 for more permeable surfaces. For example, a typical CN for asphalt pavement is 98, whereas a CN for a golf course may be 61 or less. In a typical application, a CN would be selected from a local county or SCS guidance document. However, if runoff volume, precipitation volume, and  $I_a$  are measured or determined from field work, a CN can be directly calculated.

The total depth of runoff from a storm is related to a CN by the following equations:

$$Q = \left\{ \frac{(P - I_a)^2}{[(P - I_a) + S]} \right\} \quad (2)$$

where  $Q$  is runoff volume;  $P$  is precipitation volume;  $I_a$  is initial abstraction; and  $S$  is the potential maximum retention of precipitation in the soil after runoff has begun (as runoff of precipitation occurs, some precipitation is still infiltrated, or retained, in the soil), which relates to  $I_a$  as:

$$S = \frac{I_a}{0.2} \quad (3)$$

The CN is then calculated as follows:

$$CN = \frac{1000}{(S + 10)} \quad (4)$$

These parameters were measured at the Jacob Site watershed using a PRS on September 4 and 5 and November 6 and 7 in 2008 and on March 3, April 30, and November 10 and 11 in 2009. Rainfall simulators are designed to determine the runoff and infiltration properties of field soils under non-ponded conditions. The PRS used for this study consisted of a flat Plexiglas reservoir (61 x 61 cm) for water, with hypodermic needles on the underside (Mutchler and Moldenhauer, 1963; Munn and Huntington, 1976). Water drops were produced on the needles by providing a constant gravity head, wetting a 3612 cm<sup>2</sup> area of ground directly beneath the rainfall simulator. Rainfall simulations were conducted at rates of approximately 4.17 cm/hr, the maximum intensity during a local 1-hour, 100-year storm, as per the NOAA Atlas 14 (NWS/NOAA, 2004) for the location coordinates.

To collect a one-gallon container of runoff and sediment for particle size analysis, a small trough was entrenched just downslope of the footprint of the PRS. A piece of PVC pipe, sliced lengthwise in half and capped at both ends, was placed in the trough with a 90° -bend aluminum flashing installed over the trough lip to collect the flow, which was then bailed into a 3.8-liter container. Runoff collection was stopped after one hour.

Before and after each rainfall simulation, a calibration was performed to ensure that the application rate was approximately at the target rate and to evaluate any drift from the initial rate. This was done by placing a Plexiglas plate under the PRS to collect the water output at three one-minute increments before each test, and at a minimum, at least for one one-minute increment after each test. The amount of collected output was measured in a graduated cylinder. Without flow interruption after the calibrations, the plate was quickly removed and the experiment was started. At the conclusion of the experiment, again without flow interruption, the Plexiglas plate was inserted back under the simulator, and as before, the output was captured for at least one, one-minute increment. These initial and post-calibration rates were averaged and used as the application intensity in calculations to determine infiltration properties.

In general, after the initial calibration measurements, the experimental precipitation event was started on the test surface, during which five time measurements were recorded:

(1) when initial ponding occurred anywhere on the surface test plot, (2) when initial runoff occurred anywhere on the surface test plot, (3) when runoff occurred in each quadrant of the surface test plot, and (4) when a flowpath developed from the back to the front of the surface test plot, and (5) when initial runoff reached the collection trough. The time measurements, combined with the rainfall intensity, allow an  $I_a$  value to be estimated for each measured ponding and runoff event. Once  $I_a$  is established, a CN can be calculated.

A soil sample was collected from the center of each test plot after one-hour of rainfall simulation, and a “pre-rainfall” (dry) soil sample was collected adjacent to each test plot. Soil moisture conditions were determined from these samples.

A total of six rainfall simulation tests were performed, with two test plot locations selected at each of three separate sites. At each site, one rainfall simulation test was performed on a plant mound, whereas a second test was performed in the adjacent interspace between plants. The three sites consisted of a burned ridge, a burned channel area, and an unburned control area.

## **RESULTS**

### **Meteorology**

Meteorological data were summarized by monthly average, minimum, and maximum 10-minute values. Data were lost for most of December 2008 and May 2009 as well as the first part of June 2009. Data losses were due to a combination of datalogger malfunctions and one case of operator error during data download.

Temperature and relative humidity at the Jacob site (Figure 6 and Figure 7) follow expected trends for the Great Basin, with temperatures peaking June through August (maximum values around 40 °C) and exhibiting sub-zero minima during the months of November through April. November through February have the highest average relative humidity, with March and April relative humidities also slightly elevated compared to the rest of the year. Soil temperature temporal trends (Figure 8) follow ambient temperature trends. Soil water content (Figure 9), in contrast, generally follows ambient temperature trends, but peak monthly soil water content and to a lesser extent average soil water content are clearly influenced by the amount of precipitation. For example, elevated values of peak soil water content in February and July 2009 are clearly a result of precipitation during those months. It is noteworthy in the context of the discussion of dust emissions potential as measured by PI-SWERL that September 2009 was the month with the lowest average soil suspension and maximum soil water content values.

The average and maximum 10-minute wind speeds on a monthly basis are shown in Figure 10 and a wind rose diagram illustrating the frequency and magnitude of winds from specific directions are shown in Figure 11. March through August 2009 were the windiest

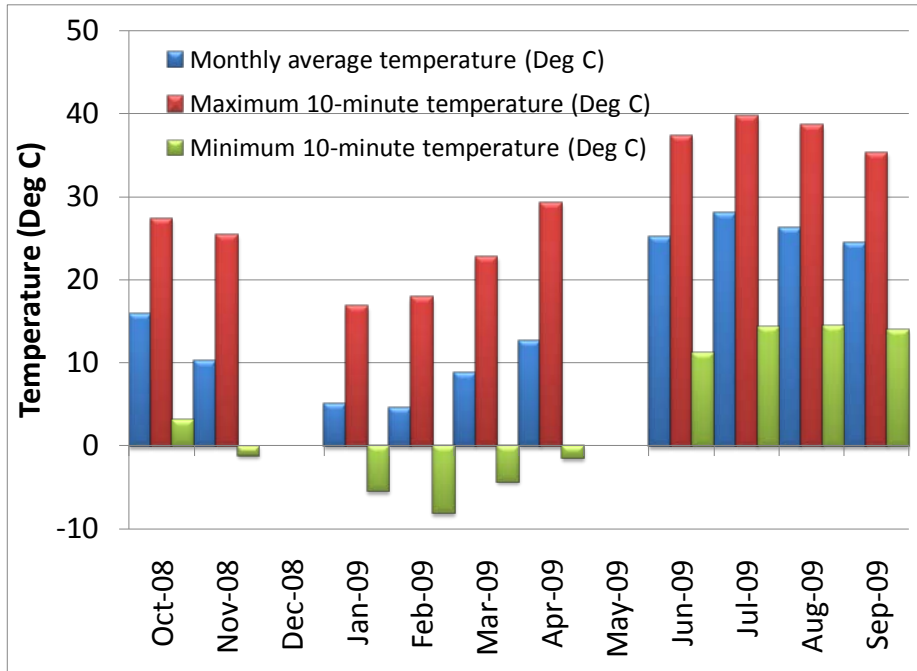


Figure 3. Monthly temperature at Jacob site.

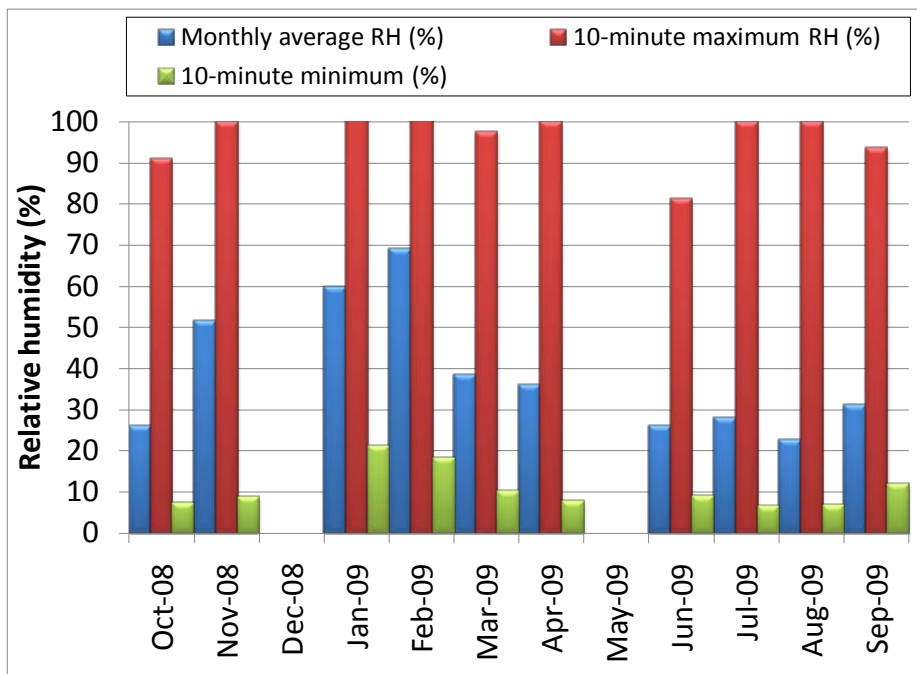


Figure 4. Monthly relative humidity at Jacob site.

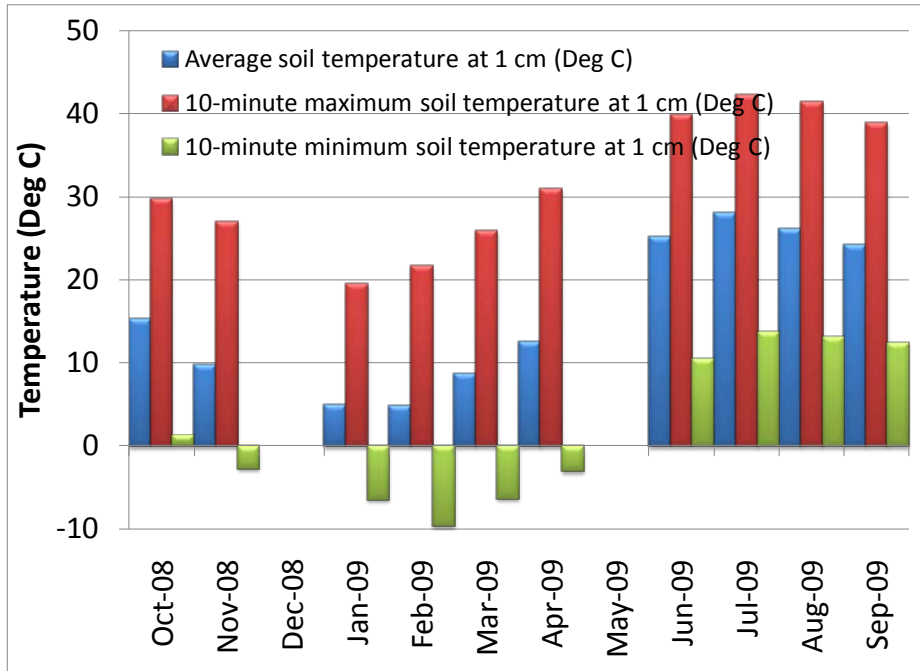


Figure 5. Temperature of soil in top 1 cm at Jacob site.

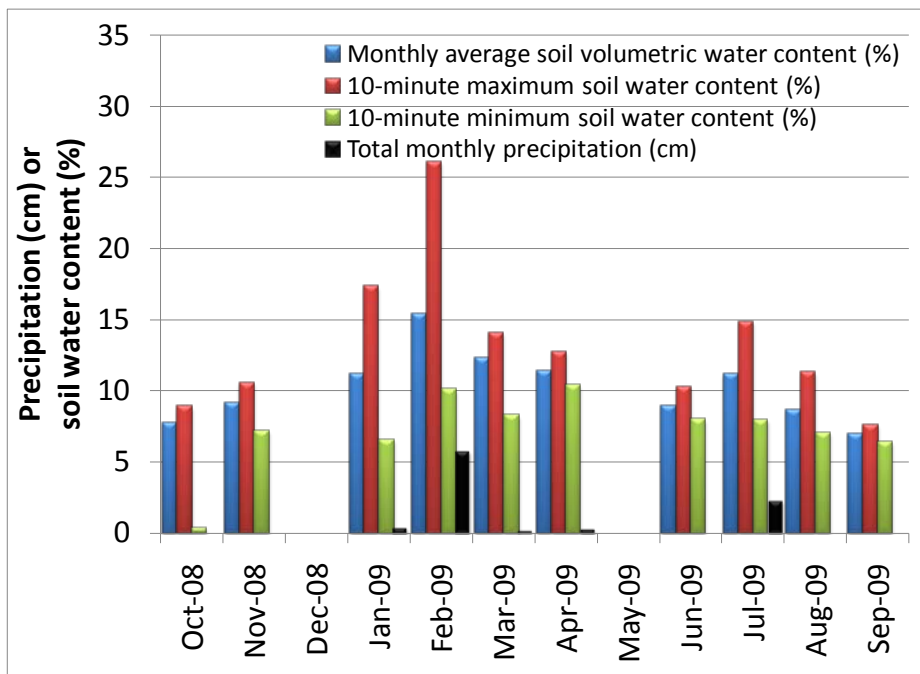


Figure 6. Monthly soil volumetric water content and total monthly precipitation (cm) at Jacob site.

months with 10-minute maximum winds near 15 m/s (33 mph) and in the case of June, 2009, near 20 m/s (45 mph). As discussed in a later section, substantial dust emissions, especially from burned areas, can occur at sustained wind speeds of as little as 11 m/s (24 mph) when the soil surface is dry enough.

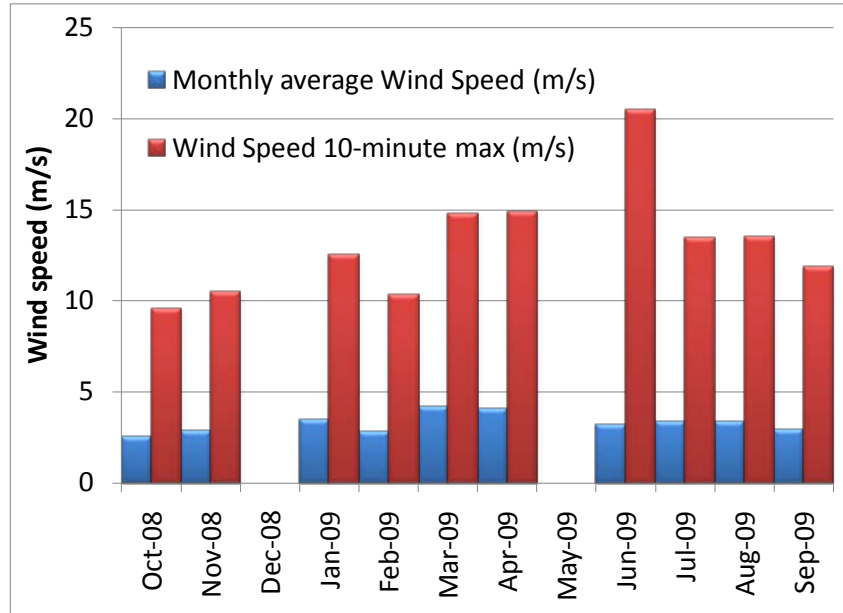


Figure 7. Monthly average and maximum wind speeds at Jacob site.

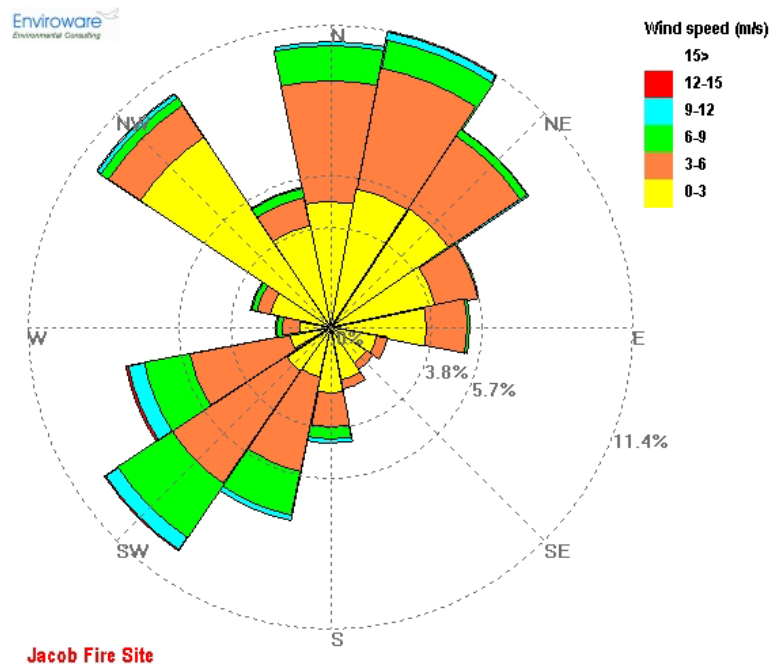


Figure 8. Wind rose from Jacob's fire site (10/08–9/09).

Surface winds at the Jacob site over the measurement period were predominantly northnortheasterly and southwesterly, with an infrequent, but notable northwestern component. Wind speeds were rarely higher than 12 m/s and were light to moderate (0–6 m/s) the majority of the time.

### PI-SWERL Measurements

Figures 12 through Figure 15 show the cumulative PM<sub>10</sub> emissions as measured by the PI-SWERL at 1, 3, 6, and 13 MAB at the Jacob fire. These data show several significant trends. First, in almost all cases, emissions from the native desert were the lowest among all of the surfaces tested. Second, emissions from charred plant mounds on burned wash surfaces were generally higher than emissions from charred plant mounds on ridges. Third, emissions from interspace areas in washes were also generally higher than emissions from interspace areas on ridges. Fourth, both for wash and ridge locations, emissions from charred plant mounds were higher, sometimes by more than an order of magnitude, than emissions from not charred interspace regions. The tests conducted at 3 (MAB) (Figure 13) differ slightly from these general trends in that emissions from burned ridge surfaces were comparable to those from native desert and emissions from plant mounds on ridge surfaces were comparable to those from interspace regions. This is attributed to the relatively high soil moisture content, as observed by field personnel, during the 3 MAB sampling effort as compared to the other three sampling times (1, 6, and 13 MAB). It is not clear why wash sites did not appear to be as affected by the increased soil moisture as ridge sites.

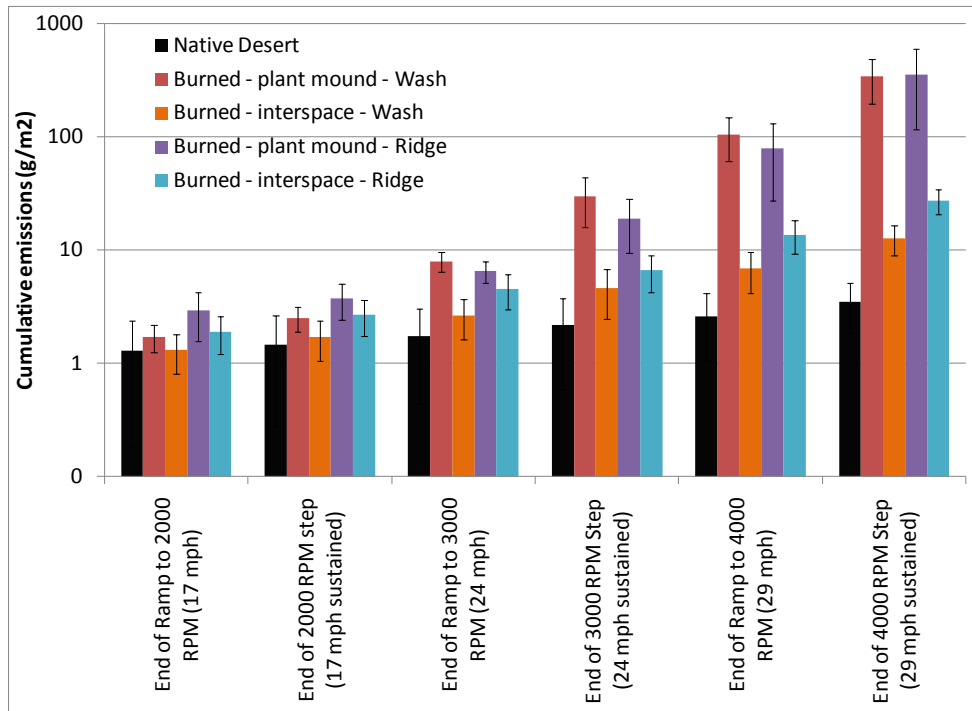


Figure 9. PI-SWERL results at 1 MAB.

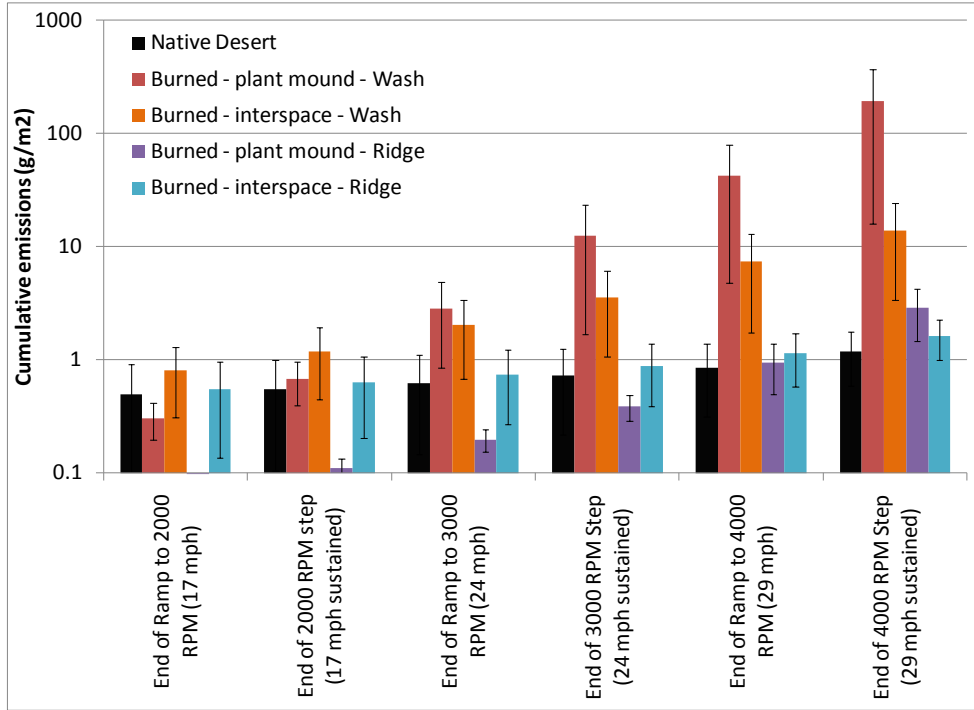


Figure 10. PI-SWERL results at 3 MAB.

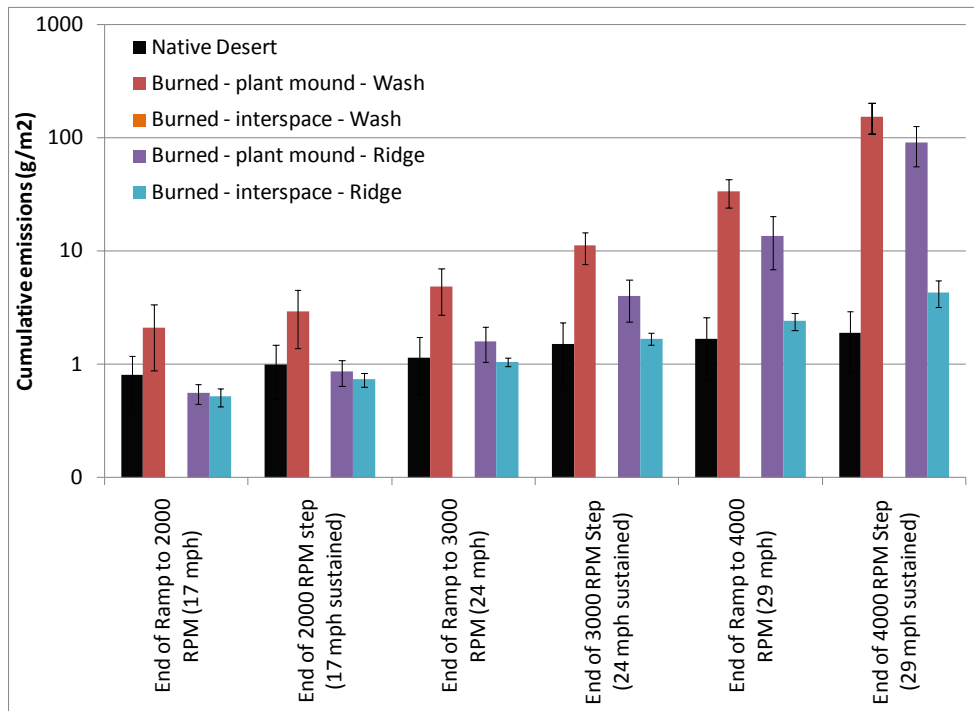


Figure 11. PI-SWERL results at 6 MAB. For measurements in the wash, only burned plant mound areas were sampled at 6 MAB.

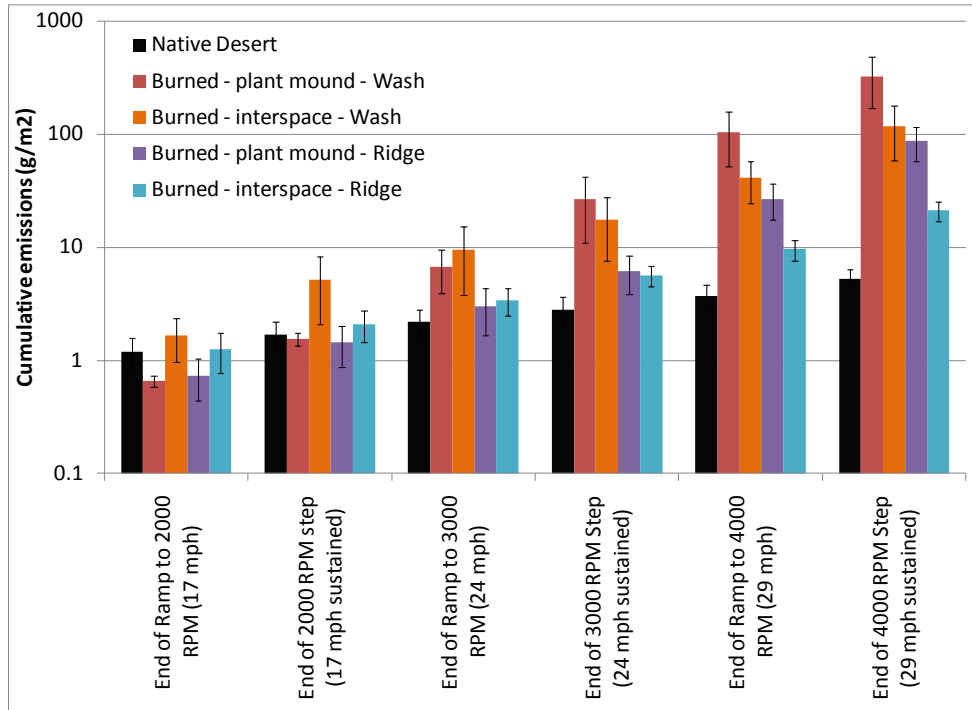


Figure 12. PI-SWERL results at 13 MAB.

Moist soil at 3 MAB notwithstanding, the relationship between  $PM_{10}$  windblown emissions and the type of surface sampled is quite clear. Areas that were subjected to fire have higher emissions than the native desert surfaces. Within areas subjected to fire, charred plant mounds have much higher emissions than what appear to be not charred interspace regions. Wash locations, charred or not charred, have higher emissions than their ridge counterparts. These observations provide a clear indication that fire causes the soil surface over the entire burned area to be more susceptible to wind erosion. However, emissions from plant mounds are especially elevated. As discussed in greater detail below, it is interesting to note that these higher  $PM_{10}$  emissions cannot be attributed solely, or even in large part, to elemental or organic carbon. In other words, it is not simply that the increased  $PM_{10}$  emissions are a result of the availability of charred plant debris. The removal of the plants by fire appears to enable the emissions of fine soil particles that had been accumulating at the base of the plants.

It is more convenient to examine the behavior of emissions over time by selecting a specific PI-SWERL RPM to compare across the four sample intervals (see Figure 16). For all surfaces tested,  $PM_{10}$  emissions at the end of the 3000 RPM step (roughly equivalent to sustained 24 mph winds) were lower at 3 MAB than the other three measurement periods (1, 6, and 13 MAB), which is consistent with the observation that the soil was visibly moist at 3 MAB. Interestingly, the native desert, charred plant mounds in wash locations, and interspaces at the ridge showed similar emissions at 1 and 13 MAB. We note that both of these measurements occurred in early fall, so it is reasonable to assume that soil conditions were similar (whereas 6 MAB was in early spring and 3 MAB was associated with a wet soil). This is expected for native desert surfaces since they were not directly affected by fire

and it is reasonable to assume that dust emissions potential would not change much from year to year. For charred wash and interspace ridge areas, this observation suggests that those surfaces did not exhibit attenuation of dust emissions over the course of one year. In contrast, dust emissions from charred plant mounds on ridges did attenuate and were comparable to those from interspace areas on ridges by 13 MAB. One explanation for this is that due to their exposure to wind and high potential for windblown emission, suspendable dust was readily depleted from charred areas on ridges. There may be other explanations that are related to how rain might serve to stabilize these interspace surfaces. In contrast, interspace areas in wash locations exhibited an increase in dust emission potential between 1 MAB and 13 MAB. This may be an indication that suspendable material from other parts of the Jacob fire site was transported by wind or water to the wash interspaces.

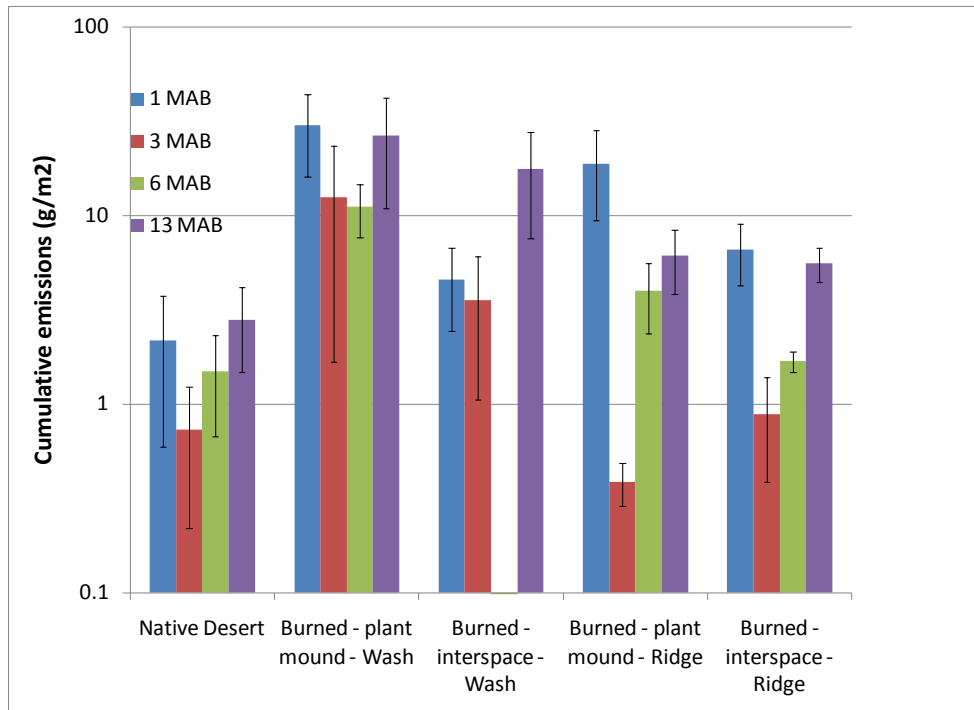


Figure 13.  $PM_{10}$  emissions at the end of the 3000 RPM Step (24 mph sustained) at 1, 3, 6, and 13 MAB.

The changes in dust emissions over time discussed above begin to provide a glimpse of the complex redistribution of materials that occurs after a fire. This redistribution, which can include suspension and transport of dust to off-site areas may have important implications for radionuclide-contaminated soils on the NTS, TTR, and NTTR. For example, some sites from which emissions would be expected to gradually diminish as the supply of particles is reduced over time, maintained elevated emissivity because of redistribution of particles within the burned area.

## Filter Samples and Analysis

Figures 17 through Figure 21 show the abundance of certain classes of compounds with respect to the total mass measured on PM<sub>10</sub> filter samples. For example, soil element abundances are calculated by dividing the sum of the masses of Al, Si, K, Ca, Ti, Fe, and Sr by the total mass of PM<sub>10</sub> material (measured independently) found on the filter. The five classes of chemicals are elements associated with mineral soil material, carbonaceous compounds (including carbonate), water-soluble anions and cations, relatively common elements, and relatively rare elements. Figures of the abundances of chemicals in each of these classes by individual constituents are provided in an Appendix to this report.

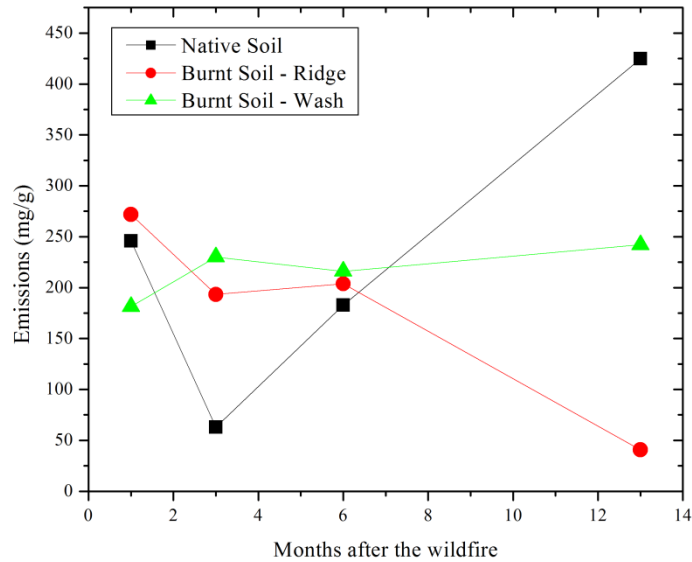


Figure 14. Abundance of elements associated with soil minerals (Al, Si, K, Ca, Ti, Fe, Sr).

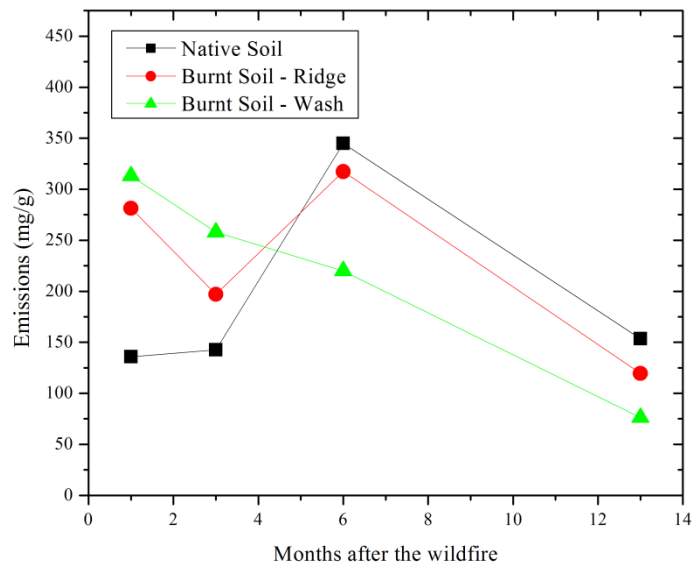


Figure 15. Abundances of carbon compounds (elemental carbon, organic carbon, and carbonate).

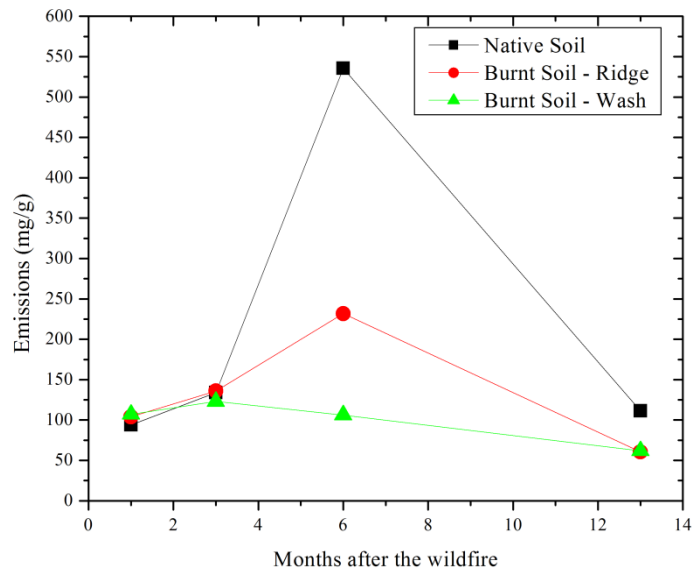


Figure 16. Abundances of water-soluble species (nitrate-  $\text{NO}_3^-$ , sulfate-  $\text{SO}_4^{2-}$ , ammonium-  $\text{NH}_4^+$ , sodium-  $\text{Na}^+$ , Magnesium-  $\text{Mg}^{2+}$ , potassium-  $\text{K}^+$ , and calcium-  $\text{Ca}^{2+}$ ).

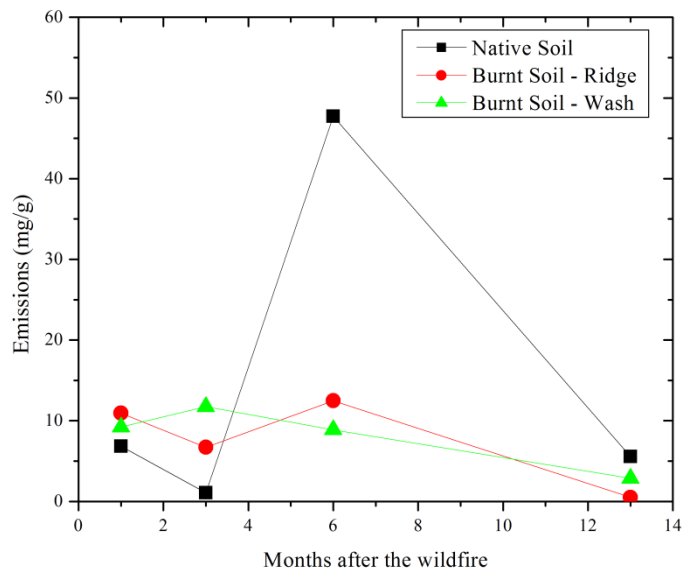


Figure 17. Abundances of common elements (Na, Mg, P, S, Cl, V, Mn, Ni, and Cu).

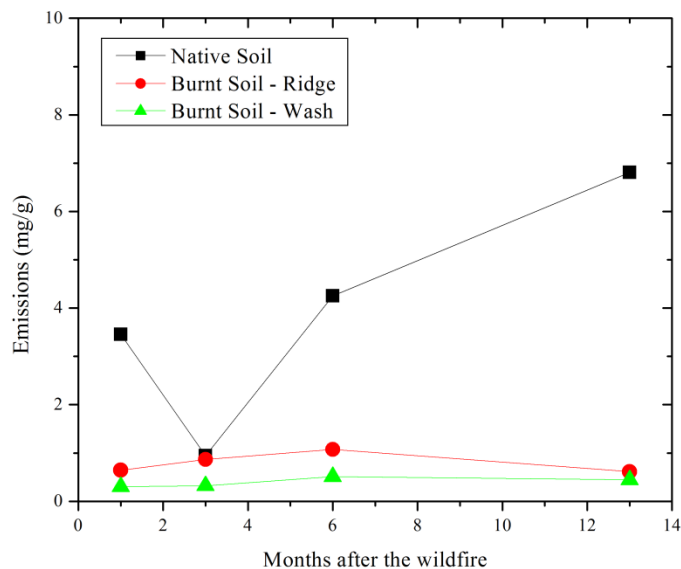


Figure 18. Abundances of rare elements (Zn, Br, Rb, Yb, Zr, Eu, Hf, Tl, and Pb).

As expected, at 1 MAB, the relative abundances of carbon-containing compounds on both burned ridge and burned wash areas are higher than those on native desert surfaces. We note here that the burned ridge and burned wash filter samples represent the combined chemical profiles of both plant mound and interspace areas. After 1 MAB, the trends in carbon-containing compounds as well as the other classes of chemicals are somewhat more complex. For example, at 3 MAB, abundances of all chemical classes seem to decrease relative to 1 MAB for native desert. It is not clear how much of this can be attributed to soil moisture effects and how much is just inherent measurement noise. Additional data will be required before meaningful assessment of long-term trends can be provided with regard to the composition of suspendable material.

### Runoff Measurements

The calculated CN data from the rainfall simulator experiments are shown in Table 1. From previous rainfall simulation studies performed on the NTS (Miller and French, 2001), it was determined that the most appropriate CN for each surface came from the “All Quadrant Runoff” measurement; however, in these tests, that value was not always obtained if runoff did not occur in all quadrants. Therefore, for the purposes of this study, the “Initial Runoff” CN value was used.

At 1 MAB (September 2008 tests), CNs for the burned areas were expected to be relatively high, as the result of probable hydrophobic soil conditions that exist post-fire. The relatively high CNs for tests on the burned surfaces are probably indicative of this condition. However, we expected to see lower CNs at the burned plant mound tests, where roots and biointrusion would have disturbed the soil structure, just as lower CN values were measured at the unburned plant mounds. The researchers noted that within two weeks of the burn when the Jacob fire site was first visited, small mammals had already returned to the area and had

Table 1. Curve numbers for the first measurements made at the Jacob Site.

Surface	Date	Curve Numbers for Rainfall Simulation Tests			
		Ponding	Initial Runoff	All Quadrant Runoff	Initial Runoff to Trough
Burned Ridge, Plant Mound	090408	92	92	No Runoff	No Runoff
	110608	96	96	93	93
	043009	94	90	84	No Runoff
	111009	97	96	92	84
Burned Ridge, Interspace	090408	93	93	88	94
	110608	98	95	89	87
	043009	95	94	93	92
	111009	88	86	84	86
Burned Channel, Plant Mound	090508	98	97	96	92
	110608	94	93	90	89
	030309	No Ponding	No Runoff	No Runoff	No Runoff
	111009	98	97	94	91
Burned Channel, Interspace	090508	No Ponding	No Runoff	No Runoff	No Runoff
	110708	No Ponding	No Runoff	No Runoff	No Runoff
	030309	No Ponding	No Runoff	No Runoff	No Runoff
	111009	No Ponding	No Runoff	No Runoff	No Runoff
Unburned, Plant Mound	090508	72	No Runoff	No Runoff	No Runoff
	110708	94	92	92	92
	043009	96	93	91	90
	111009	93	84	84	83
Unburned, Interspace	090508	96	95	93	93
	110708	92	91	87	86
	043009	95	92	91	90
	111109	99	98	95	93

burrowed into the now burned plant mounds. However, the CN numbers at burned plant mounds were fairly high (92, 98), indicating perhaps that hydrophobic material from the burn event served to decrease infiltration, despite disturbance associated with roots and biointrusion. There was no ponding or runoff recorded at the burned channel interspace test plot. The soil in the channel was loose sand and gravel, typical of channel beds, and was not expected to produce much runoff. In contrast, at the unburned interspace test plot, where a well-developed desert pavement existed, curve numbers were relatively high.

During subsequent tests (3–13 MAB), changes in runoff potential occurred over time at some of test plots. Interspace test plots at the burned channel did not exhibit any ponding or runoff at any time. At the burned channel, plant mound test plots, the CN decreased during the first six months, suggesting that the burned plant contributed to the initial hydrophobicity of the soil; however, at the one year test, the CN had again increased. One hypothesis for this trend is at a lower intensity fire such as at Jacob, the burn may have weakened but not caused the soil structure to collapse. However, with time, soil collapse may have gradually occurred, increasing soil bulk density, a condition usually resulting in increased runoff (measured here by an increase in the CN). Although soil bulk density measurements were not initially made at the Jacob fire site, an effort is being made to reconstruct these values from samples collected for soil texture and moisture content analysis. In future efforts, bulk density measurements will be taken to test this hypothesis. However, the burned ridge, interspace test plots have continuously had runoff values approximately the same as the unburned, interspace test plots, suggesting that the fire was not hot enough to change the soil structure in the interspace areas.

### Moisture Content

Moisture content sampling during PRS tests showed post-rain moisture contents increasing between 4 to 14 times the in-situ moisture content of each test plot (Table 2). In-situ soil moisture values were approximately the same for all test plots. However, moisture content increases were largest on the plant mound plots post-rainfall.

### Collected Runoff Volumes and Particle Sizes

To determine runoff volumes, hydrographs, and sediment particle sizes that were transported by runoff, any runoff that occurred during rainfall simulation tests was collected. Runoff hydrographs from each site, over time, are shown in Figures 22 through Figure 24. Results of laboratory analyses of the particle sizes contained within the collected runoff for the first two sampling intervals are shown in Figures 25 and Figure 26. Additional analysis of samples from later events is still on-going, and thus results are not reported here. This information can be used to determine if increasing time from the fire affects the particle sizes and volumes of sediment being transported by runoff.

Figure 25a indicates that as fines were significantly removed from the burned plant mounds, allowing for larger particles to be transported. A similar effect is seen on the unburned plant mound (Figure 25b), which may be a seasonal effect of vegetative cover loss or a weather-related effect. Regardless, the effect is significantly more pronounced at the burned plant mound. At the burned ridge interspace test plots, the effect of the fines being removed from the system is very apparent in Figure 26a. As there is no burned vegetation or

root system in place to hold the soil in place or to block the wind, the fines have been significantly eroded from the burned ridge. This same effect is not seen at the unburned interspace (Figure 26b), where the site is protected by surrounding vegetation.

Table 2. Moisture content results of in-situ (initial) vs. post-rain (final) soils.

Surface	Date	Gravimetric Moisture Content	
		Initial Moisture Content	Final Moisture Content
Burned Ridge, Plant Mound	090408	0.02	0.19
	110608	0.02	0.18
	043009	0.06	0.14
	111009	0.02	0.20
Burned Ridge, Interspace	090408	0.02	0.09
	110608	0.07	0.13
	043009	0.09	0.10
	111009	0.01	0.12
Burned Channel, Plant Mound	090508	0.01	0.14
	110708	0.04	0.14
	030209	0.12	0.14
	111009	0.03	0.15
Burned Channel, Interspace	090508	0.01	0.10
	110608	0.05	0.13
	030209	0.02	0.16
	111009	0.01	0.11
Unburned, Plant Mound	090508	0.02	0.14
	110708	0.05	0.12
	043009	0.03	0.11
	111009	0.02	0.13
Unburned, Interspace	090508	0.01	0.08
	110708	0.05	0.13
	043009	0.06	0.15
	111109	0.01	0.11

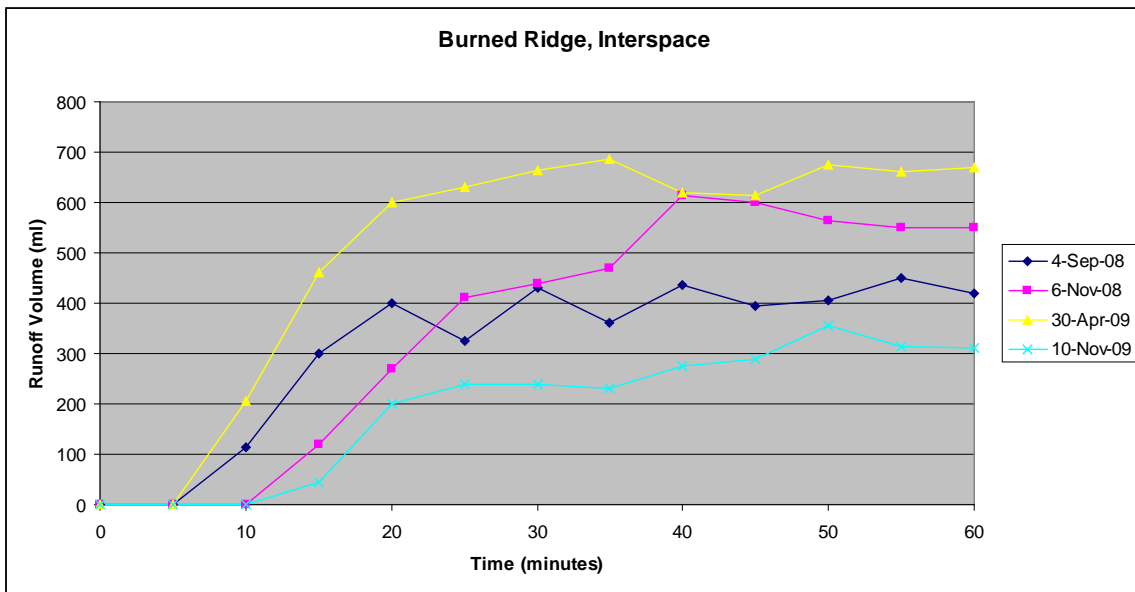


Figure 19. Runoff hydrographs from the various test plots, over time, at Jacob Fire site. A: Burned Ridge, Plant Mound. B: Burned Ridge, Interspace

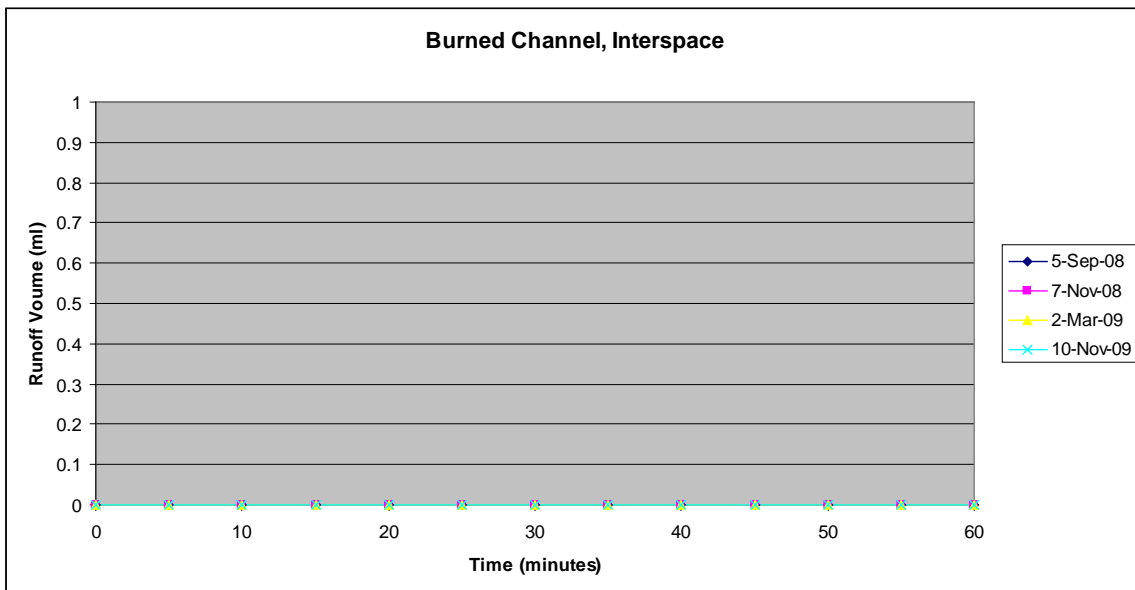
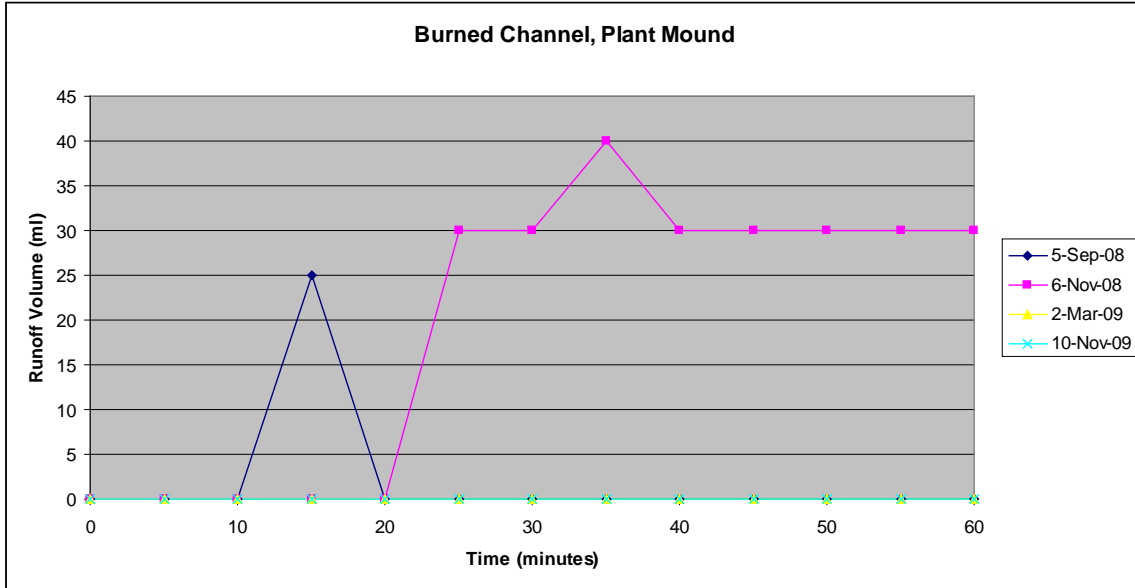


Figure 20. Runoff hydrographs from the various test plots, over time, at Jacob Fire site. C: Burned Channel, Plant Mound. D: Burned Channel, Interspace.

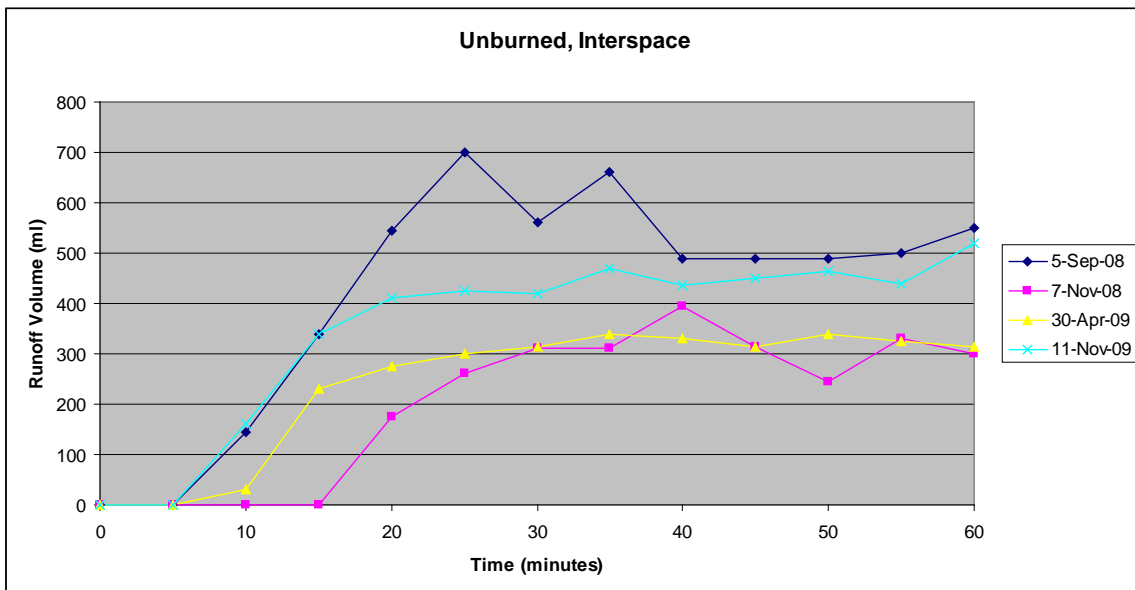
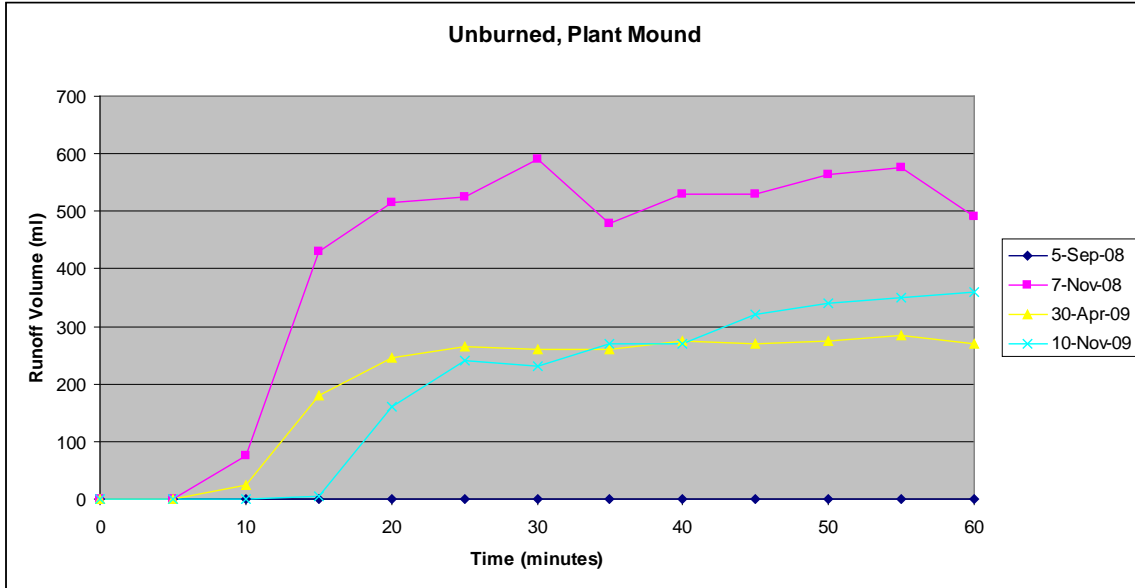


Figure 21. Runoff hydrographs from the various test plots, over time, at Jacob Fire site. E: Unburned, Plant Mound. F: Unburned, Interspace.

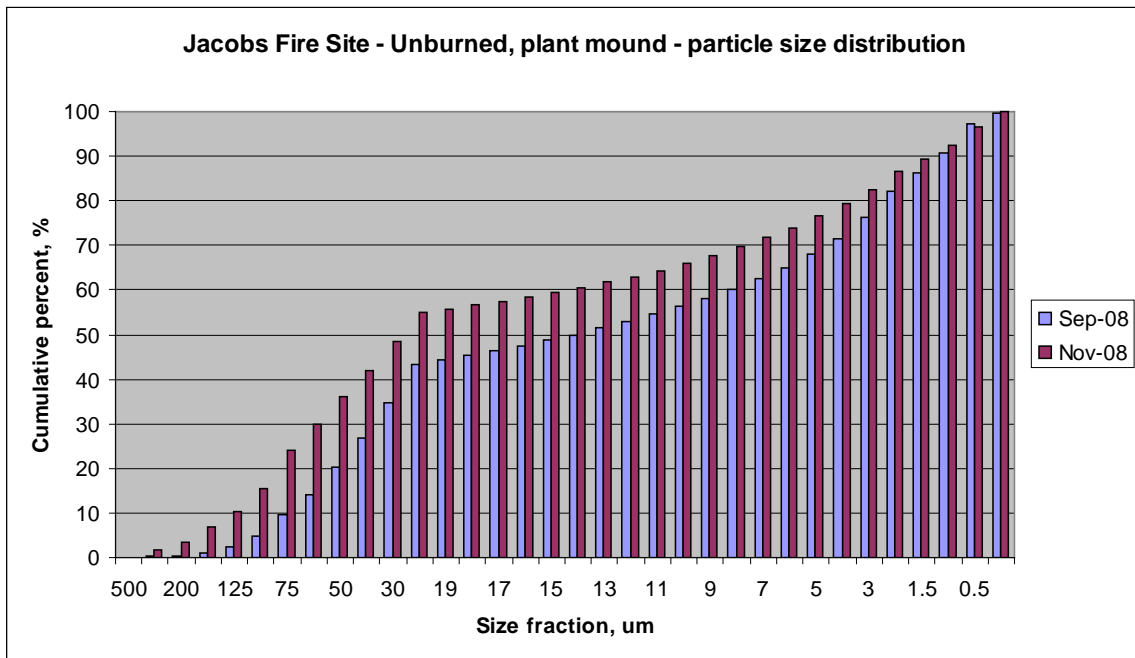
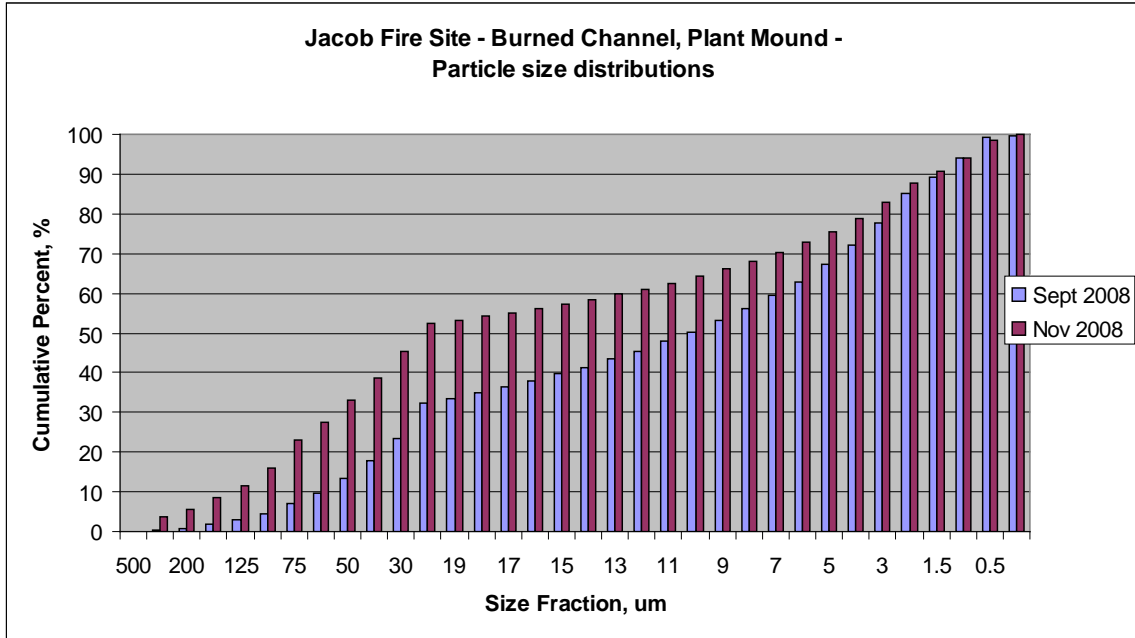


Figure 22. Comparison of particle size distributions at the burned channel plant mound and burned ridge interspace test plots between September 2008 and November 2008 sampling events.

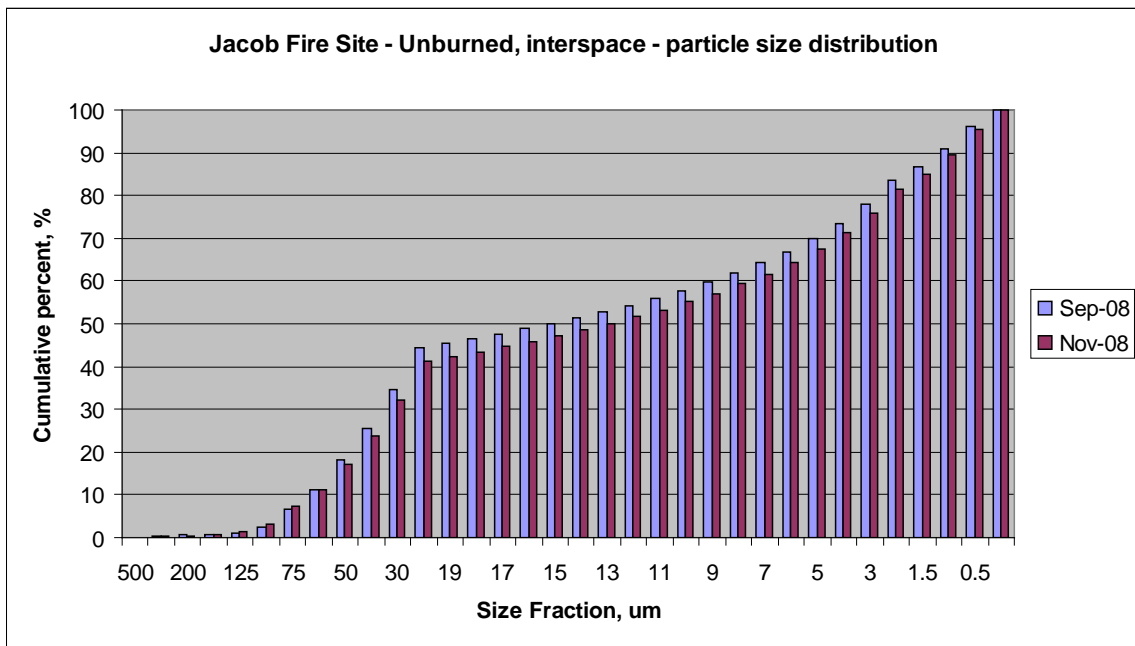
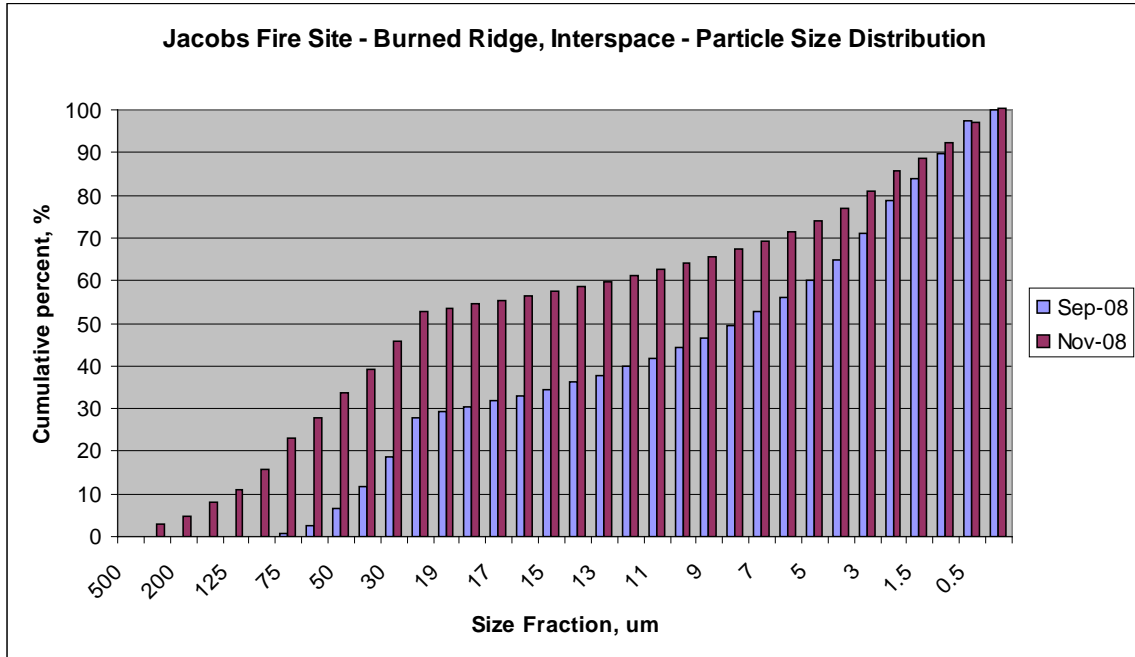


Figure 23. Comparison of particle size distributions at the burned and unburned interspace test plots between September 2008 and November 2008 sampling events.

## PRELIMINARY CONCLUSIONS

After the first year of measurements at the Jacob fire site, several preliminary trends were observed, although we note that the measurements also indicate that there are substantial seasonal influences on almost all parameters measured and firm conclusions regarding long-term trends are not appropriate at this time. PI-SWERL measurements indicated quite consistently that the potential for PM<sub>10</sub> windblown dust emissions was higher on areas that were burned compared to areas that were not. Among the burned areas, charred plant mounds located in washes were the most emissive, and interspace areas between plant mounds along burned ridges were least emissive. Comparing measurements at 1 and 13 months after the burn — when environmental conditions are likely to be similar — there remain substantial differences in emissions between burned and unburned areas, indicating that the effects of the fire have not been dampened by the passage of one year.

Preliminary analysis of PM<sub>10</sub> filter samples collected from the PI-SWERL exhaust indicates that, as expected, the fraction of PM<sub>10</sub> attributable to carbon one month after the fire was higher on burned areas than the surrounding native desert. Extraction of longer-term or more subtle trends will require additional data to be considered.

Rainfall simulation measurements at the Jacob fire site suggested that fire may have a complex effect on infiltration and runoff. Some burned surfaces initially (1 month after fire) exhibited high curve numbers (indicating high runoff potential) followed by lower curve numbers (at 3 and 6 months after the fire), with a return to higher curve numbers at 13 months after the fire. Noting that this observation is based on a limited dataset, one possible hypothesis to explain this behavior is that post-fire runoff may have been initially most influenced by hydrophobicity that reduced soil infiltration and increased runoff. In later months, the hydrophobic effect was reduced, and the soil that was loosened by the fire was comparatively easier for water to infiltrate into. As more time passed, the soil structure collapsed, reducing pore spaces, increasing bulk density and reducing infiltration capacity. Longer-term measurements as well as measurements at other fire sites will assist in developing this and other hypotheses regarding soil behavior after a fire event.

An update to this report will be provided after measurements at the Jacob site are completed on the 2-year anniversary of the fire.

## REFERENCES

- Brooks, M. 2006. Ecology and management of fire in the Mojave Desert. Abstracts with Program, Nevada Wildland Fire Research and Outreach Conference. Reno, NV.
- Chambers, J.C., N. Devoe, and A. Evenden (eds.). 2008. Collaborative management and research in the Great Basin. General Technical Report RMRS-GTR-204, Fort Collins, 66p.
- Hansen, D.J. and W.K. Ostler, 2004. A Survey of vegetation and wildland fire hazards on the Nevada Test Site. Bechtel Nevada Ecological Services, DOE/NV/11718-981. 57pp.
- Hunter, R.H. 1991. *Bromus* invasions on the Nevada Test Site: present status of *B. rubens* and *B. tectorum* with notes on their relationship to disturbance and altitude. *Great Basin Naturalist* 52 (2) pp. 176-182.
- Knapp, P.A. 1996. Cheatgrass (*Bromus tectorum* L) dominance in the Great Basin. *Global Environmental Change* 6 (1), pp. 37-52.
- National Interagency Coordination Center. 2006. Annual fire summary 2005. National Interagency Fire Coordination Center, Boise. 15pp.
- National Nuclear Security Administration. 2005. Fire at Nevada Test Site 100 Percent Contained. Nevada Site Office News Press Release, June 9, 2005.
- Neary, D.G., C.C. Klopatek, L.F. DeBano and P.F. Ffolliott. 1999. Fire effects on belowground sustainability: a review and synthesis. *For. Ecol. Manage.* 122:51-71.
- Ostler, W.K., D.J. Hansen, D.C. Anderson, and D.B. Hall. 2000. Classification of Vegetation on the Nevada Test Site. DOE/NV/11718-477. Bechtel Nevada Ecological Services, Las Vegas. Paginated by Section.
- Rickard, W.H. and J.C. Beatley. 1965. Canopy-coverage of the desert shrub vegetation mosaic of the Nevada Test Site. *Ecology*, 46, 524-529.
- Savage, M. and T.W. Swetnam. 1990. Early 19th-century fire decline following sheep pasturing in a Navajo ponderosa pine forest. *Ecol.* 71:2374-378.
- Shafer, D.S., D. DuBois, V. Etyemezian, J. Xu, I. Kavouras, J.J. Miller, G. Nikolich, and M. Stone. 2007. Fire as a long term stewardship issue for soils contaminated with radionuclides in the western United States. Proceedings of the 11<sup>th</sup> International Conference on Environmental Remediation and Radioactive Waste Management. Bruges, Belgium.
- Shafer, D.S. and J. Gomes. 2009. Plant mounds as concentration and stabilization agents for actinides in soil. Proceedings of Waste Management 2009, 49 (4) Phoenix.
- Sugihara, N.G. 2006. Fire in California's Ecosystems. University of California Press. 596 pp.
- Taylor, W.J. and J.M. Bartley. 2002. Prevolcanic extensional Seaman breakaway fault and its geologic implications for eastern Nevada and western Utah. *GSA Bulletin* 104 (3): 255-266.

- Westerling, A.L. and T.W. Swetnam. 2003. Interannual to decadal drought and wildfire in the western United States. *EOS* 84:545–560.
- Westerling, A.L., H.G. Hidalgo, D.R. Cayan, and T.W. Swetnam. 2006. Warming and earlier spring increases western U.S. forest fire activity. *Science* 313: 940 – 943.
- Clark County Regional Flood Control District (CCRFCD), 1999. *Hydrologic Criteria and Drainage Design Manual*. Las Vegas, Nevada.
- Hjelmfelt, A.T. 1991. *Investigation of Curve Number Procedure*. Journal of Hydraulic Engineering, Vol. 117, No. 6, p. 725-737.
- Miller, J.J. and R.H. French, 2001. *Watershed Responses in Arid Environments*. American Society of Civil Engineers, Environmental and Water Resources Institute, Conference Proceedings, Annual Conference, 2001, Orlando, Florida.
- Munn, J.R. and G.L. Huntington. 1976. *A Portable Rainfall Simulator for Erodibility and Infiltration Measurements in Rugged Terrain*. Soil Science Society of America Journal, Vol. 40, p. 622-624.
- Mutchler, C.K. and W.C. Moldenhauer. 1963. *Applicator for Laboratory Rainfall Simulator*. Transactions of American Society of Agricultural Engineers, Vol. 6, p. 220-222.
- National Weather Service/National Oceanic Atmospheric Administration. 2004. ONLINE. [www.hdsc.nws.noaa.gov](http://www.hdsc.nws.noaa.gov).
- U.S. Department of Agriculture, Soils Conservation Survey, USDA-SCS. 1986. *National Engineering Handbook - Section 4, Hydrology*. National Technical Information Service, Washington, D.C.
- Water Resources Council (WRC). 1981. *Guidelines for determining flood flow frequency*. Bulletin 17b, U.S. Water Resources Council, Washington, D.C.

## APPENDIX: SUPPLEMENTAL DATA

Table A-1. Emissions profiles of PM<sub>10</sub> components emitted from unburned and burnt soils after one month from the fire event

	Unburned	Burnt (Ridge)	Burnt (Wash)
Chloride, Cl <sup>-</sup>	1.571 ± 6.733	0.285 ± 0.217	0.241 ± 0.204
Nitrate, NO <sub>3</sub> <sup>-</sup>		0.253 ± 0.218	0.286 ± 0.204
Sulfate, SO <sub>4</sub> <sup>2-</sup>	5.029 ± 6.748	8.533 ± 0.223	9.747 ± 0.212
Ammonium, NH <sub>4</sub> <sup>+</sup>	1.8 ± 6.783	0.219 ± 0.221	0.219 ± 0.207
Sodium, Na <sup>+</sup>	2.371 ± 0.544	0.484 ± 0.046	2.027 ± 0.178
Magnesium, Mg <sup>2+</sup>	7.886 ± 0.75	4.579 ± 0.105	4.723 ± 0.108
Potassium, K <sup>+</sup>	2.6 ± 0.712	2.979 ± 0.079	3.461 ± 0.091
Calcium, Ca <sup>2+</sup>	74.114 ± 7.278	86.929 ± 1.261	86.596 ± 1.252
Total OC	92.752 ± 62.186	73.5 ± 5.186	108.563 ± 6.8
Total EC	16.314 ± 12.923	123.25 ± 6.458	110.603 ± 5.806
Carbonate, CO <sub>3</sub> <sup>2-</sup>	26.867 ± 59.322	84.608 ± 5.725	93.831 ± 6.076
Total Carbon	135.933 ± 92.092	281.358 ± 12.809	312.998 ± 13.869
Sodium, Na		4.305 ± 0.688	3.538 ± 0.637
Magnesium, Mg	0.867 ± 9.814	3.625 ± 0.336	2.756 ± 0.312
Aluminum, Al	20.543 ± 2.451	10.12 ± 0.109	5.911 ± 0.079
Silicon, Si	69.21 ± 6.301	28.171 ± 0.236	15.57 ± 0.146
Phosphorous, P		0.965 ± 0.038	1.318 ± 0.037
Sulfur, S	3.629 ± 1.639	0.831 ± 0.055	0.786 ± 0.051
Chlorine, Cl	0.924 ± 0.371	0.113 ± 0.012	0.08 ± 0.011
Potassium, K	22.314 ± 1.95	14.846 ± 0.06	8.559 ± 0.036
Calcium, Ca	84.124 ± 7.333	194.43 ± 0.689	139.414 ± 0.479
Scandium, Sc	0.01 ± 1.39		
Titanium, Ti	4.038 ± 0.426	1.858 ± 0.012	0.943 ± 0.009
Vanadium, V		0.03 ± 0.001	0.013 ± 0.001
Chromium, Cr			
Manganese, Mn	1.429 ± 0.483	1.008 ± 0.017	0.698 ± 0.015
Iron, Fe	45.143 ± 3.925	21.38 ± 0.085	10.417 ± 0.045
Cobalt, Co			
Nickel, Ni		0.004 ± 0.004	
Copper, Cu		0.063 ± 0.006	0.035 ± 0.006
Zinc, Zn	0.924 ± 0.242	0.225 ± 0.008	0.086 ± 0.007

	<b>Unburned</b>	<b>Burnt (Ridge)</b>	<b>Burnt (Wash)</b>
Gallium, Ga			
Arsenic, As			
Selenium, Se	0.019 ± 0.466		0.001 ± 0.025
Bromine, Br	0.952 ± 0.343	0.109 ± 0.011	0.061 ± 0.01
Rubidium, Rh	0.19 ± 0.238	0.089 ± 0.008	0.038 ± 0.007
Strontium, Sr	0.41 ± 0.44	1.054 ± 0.016	0.654 ± 0.014
Yttrium, Y		0.029 ± 0.011	
Zirconium, Zr	0.038 ± 0.77	0.112 ± 0.025	0.083 ± 0.024
Niobium, Nb	0.162 ± 0.591		
Molybdenum, Mo			
Palladium, Pd	0.343 ± 1.01		
Silver, Ag	0.01 ± 0.97	0.01 ± 0.031	
Cadmium, Cd			
Indium, In		0.004 ± 0.021	
Tin, Sn			
Antimony, Sb			
Cesium, Cs			
Barium, Ba			
Lanthanum, La			
Cerium, Ce	0.048 ± 0.288		
Samarium, Sa			
Europium, Eu		0.018 ± 0.048	
Terbium, Tb			
Hafnium, Hf	0.467 ± 3.155		
Tantalum, Ta			
Tungsten, W			
Iridium, Ir			
Gold, Au	0.438 ± 1.743		
Mercury, Hg			
Thallium, Th			
Lead, Pb	0.886 ± 0.586	0.063 ± 0.019	0.035 ± 0.018
Uranium, U	0.038 ± 0.941	0.012 ± 0.03	0.008 ± 0.028

Table A-2. Emissions profiles of PM<sub>10</sub> components emitted from unburned and burnt soils after three months from the fire event

	<b>Unburned</b>	<b>Burnt (Ridge)</b>	<b>Burnt (Wash)</b>
Chloride, Cl <sup>-</sup>		0.302 ± 0.837	1.764 ± 0.589
Nitrate, NO <sub>3</sub> <sup>-</sup>	3.792 ± 2.138	1.581 ± 0.844	0.448 ± 0.361
Sulfate, SO <sub>4</sub> <sup>2-</sup>	6.181 ± 2.16	3.817 ± 0.88	3.916 ± 0.469
Ammonium, NH <sub>4</sub> <sup>+</sup>	0.292 ± 2.09	0.427 ± 0.826	0.23 ± 0.358
Sodium, Na <sup>+</sup>	3.334 ± 1.938	1.623 ± 0.775	0.622 ± 0.317
Magnesium, Mg <sup>2+</sup>	3.383 ± 0.271	2.434 ± 0.178	2.921 ± 0.21
Potassium, K <sup>+</sup>	3.888 ± 1.944	2.248 ± 0.783	1.572 ± 0.334
Calcium, Ca <sup>2+</sup>	112.912 ± 9.108	123.838 ± 9.191	113.33 ± 8.281
Total OC	105.626 ± 56.936	99.829 ± 47.635	70.413 ± 32.98
Total EC	31.665 ± 5.105	64.269 ± 6.884	101.447 ± 10.532
Carbonate, CO <sub>3</sub> <sup>2-</sup>	5.161 ± 18.106	32.982 ± 10.424	86.01 ± 20.035
Total Carbon	142.452 ± 38.131	197.08 ± 41.982	257.871 ± 53.06
Sodium, Na		1.689 ± 2.321	5.698 ± 1.171
Magnesium, Mg		3.281 ± 1.235	3.051 ± 0.577
Aluminum, Al	3.495 ± 0.592	12.541 ± 0.948	6.724 ± 0.495
Silicon, Si	12.208 ± 1.154	37.076 ± 2.727	18.194 ± 1.316
Phosphorous, P			1.892 ± 0.149
Sulfur, S	0.938 ± 0.465	0.851 ± 0.192	0.238 ± 0.081
Chlorine, Cl	0.023 ± 0.113	0.147 ± 0.047	0.082 ± 0.021
Potassium, K	4.955 ± 0.408	13.771 ± 1.002	10.79 ± 0.772
Calcium, Ca	24.368 ± 1.969	104.305 ± 7.577	180.01 ± 12.869
Scandium, Sc		0.023 ± 0.164	
Titanium, Ti	1.034 ± 0.113	2.209 ± 0.164	1.145 ± 0.083
Vanadium, V	0.026 ± 0.007	0.035 ± 0.004	0.011 ± 0.001
Chromium, Cr	0.038 ± 0.069		
Manganese, Mn		0.664 ± 0.077	0.727 ± 0.058
Iron, Fe	16.782 ± 1.344	22.941 ± 1.67	12.393 ± 0.888
Cobalt, Co			
Nickel, Ni		0.009 ± 0.014	0.009 ± 0.006
Copper, Cu	0.096 ± 0.062	0.043 ± 0.024	0.03 ± 0.01
Zinc, Zn	0.264 ± 0.076	0.232 ± 0.033	0.104 ± 0.014
Gallium, Ga			
Arsenic, As			

	<b>Unburned</b>	<b>Burnt (Ridge)</b>	<b>Burnt (Wash)</b>
Selenium, Se			
Bromine, Br	0.101 ± 0.103	0.113 ± 0.042	
Rubidium, Rh	0.036 ± 0.075	0.061 ± 0.03	0.059 ± 0.013
Strontium, Sr	0.219 ± 0.137	0.452 ± 0.064	0.833 ± 0.064
Yttrium, Y	0.219 ± 0.103	0.02 ± 0.04	
Zirconium, Zr		0.103 ± 0.095	0.031 ± 0.041
Niobium, Nb			0.002 ± 0.027
Molybdenum, Mo	0.11 ± 0.163		
Palladium, Pd		0.039 ± 0.123	
Silver, Ag			
Cadmium, Cd			
Indium, In			0.004 ± 0.039
Tin, Sn			
Antimony, Sb	0.445 ± 0.546		
Cesium, Cs			
Barium, Ba			
Lanthanum, La			
Cerium, Ce			
Samarium, Sa			0.009 ± 0.021
Europium, Eu		0.091 ± 0.176	
Terbium, Tb			
Hafnium, Hf	0.275 ± 0.975	0.19 ± 0.387	0.09 ± 0.168
Tantalum, Ta	0.224 ± 0.819		0.051 ± 0.14
Tungsten, W	0.323 ± 1.192	0.168 ± 0.472	0.05 ± 0.203
Iridium, Ir	0.089 ± 0.252		
Gold, Au		0.016 ± 0.215	
Mercury, Hg			
Thallium, Th	0.048 ± 0.172	0.056 ± 0.067	
Lead, Pb			0.037 ± 0.031
Uranium, U			0.043 ± 0.05

Table A-3. Emissions profiles of PM<sub>10</sub> components emitted from unburned and burnt soils after six month from the fire event

	<b>Unburned</b>	<b>Burnt (Ridge)</b>	<b>Burnt (Wash)</b>
Chloride, Cl <sup>-</sup>		0.168 ± 0.805	4.162 ± 1.047
Nitrate, NO <sub>3</sub> <sup>-</sup>	29.146 ± 19.887	1.13 ± 0.807	0.527 ± 0.222
Sulfate, SO <sub>4</sub> <sup>2-</sup>	181.687 ± 53.936	37.479 ± 2.987	9.467 ± 0.745
Ammonium, NH <sub>4</sub> <sup>+</sup>	2.913 ± 17.999	0.209 ± 0.795	0.174 ± 0.214
Sodium, Na <sup>+</sup>	153.965 ± 46.298	26.92 ± 2.179	4.881 ± 0.417
Magnesium, Mg <sup>2+</sup>	6.254 ± 1.76	3.445 ± 0.252	2.385 ± 0.17
Potassium, K <sup>+</sup>	31.731 ± 19.276	2.503 ± 0.759	1.517 ± 0.229
Calcium, Ca <sup>2+</sup>	129.967 ± 36.398	160.068 ± 11.862	87.166 ± 6.329
Total OC	227.021 ± 213.752	111.648 ± 52.791	61.246 ± 27.956
Total EC	86.024 ± 40.483	154.192 ± 16.155	111.527 ± 11.521
Carbonate, CO <sub>3</sub> <sup>2-</sup>	31.752 ± 155.925	51.48 ± 13.721	47.2 ± 11.014
Total Carbon	344.797 ± 210.225	317.319 ± 66.075	219.974 ± 44.879
Sodium, Na		2.373 ± 2.258	2.845 ± 0.68
Magnesium, Mg		1.748 ± 1.168	2.603 ± 0.376
Aluminum, Al	8.576 ± 5.019	10.602 ± 0.807	7.811 ± 0.563
Silicon, Si	58.105 ± 17.005	35.522 ± 2.61	22.26 ± 1.593
Phosphorous, P		0.119 ± 0.128	0.889 ± 0.073
Sulfur, S	46.594 ± 13.592	6.635 ± 0.521	1.24 ± 0.102
Chlorine, Cl	1.062 ± 1.027	0.652 ± 0.066	0.269 ± 0.023
Potassium, K	25.203 ± 7.082	13.944 ± 1.013	11.179 ± 0.795
Calcium, Ca	43.899 ± 12.689	121.103 ± 8.787	157.535 ± 11.192
Scandium, Sc			
Titanium, Ti	4.195 ± 1.334	1.839 ± 0.138	1.402 ± 0.1
Vanadium, V		0.033 ± 0.004	0.031 ± 0.002
Chromium, Cr			
Manganese, Mn		0.904 ± 0.088	0.958 ± 0.07
Iron, Fe	42.048 ± 11.827	20.301 ± 1.477	15.148 ± 1.077
Cobalt, Co			
Nickel, Ni	0.077 ± 0.298		
Copper, Cu		0.019 ± 0.023	0.043 ± 0.007
Zinc, Zn		0.292 ± 0.035	0.157 ± 0.014
Gallium, Ga			
Arsenic, As			

	<b>Unburned</b>	<b>Burnt (Ridge)</b>	<b>Burnt (Wash)</b>
Selenium, Se			
Bromine, Br		0.244 ± 0.043	0.084 ± 0.012
Rubidium, Rh	0.679 ± 0.672	0.053 ± 0.029	0.068 ± 0.009
Strontium, Sr	0.657 ± 1.185	0.533 ± 0.065	0.734 ± 0.054
Yttrium, Y		0.045 ± 0.039	0.007 ± 0.011
Zirconium, Zr		0.056 ± 0.091	0.088 ± 0.026
Niobium, Nb			
Molybdenum, Mo			
Palladium, Pd			
Silver, Ag	0.931 ± 2.488		
Cadmium, Cd			
Indium, In			
Tin, Sn		0.07 ± 0.103	0.01 ± 0.027
Antimony, Sb			
Cesium, Cs			
Barium, Ba			
Lanthanum, La			
Cerium, Ce			
Samarium, Sa	0.022 ± 1.056		
Europium, Eu	0.876 ± 3.818	0.126 ± 0.17	0.01 ± 0.044
Terbium, Tb			
Hafnium, Hf	0.493 ± 8.404	0.236 ± 0.372	0.066 ± 0.1
Tantalum, Ta			
Tungsten, W	1.183 ± 10.236	0.351 ± 0.455	0.097 ± 0.122
Iridium, Ir			
Gold, Au			
Mercury, Hg			
Thallium, Th	0.953 ± 1.491		
Lead, Pb	1.249 ± 1.572	0.021 ± 0.067	0.031 ± 0.018
Uranium, U	1.008 ± 2.546	0.02 ± 0.112	

Table A-4. Emissions profiles of PM<sub>10</sub> components emitted from unburnt and burnt soils after thirteen months from the fire event

	<b>Unburned</b>	<b>Burnt (Ridge)</b>	<b>Burnt (Wash)</b>
Chloride, Cl <sup>-</sup>			
Nitrate, NO <sub>3</sub> <sup>-</sup>			0.161 ± 0.147
Sulfate, SO <sub>4</sub> <sup>2-</sup>	2.143 ± 16.838		2.068 ± 0.149
Ammonium, NH <sub>4</sub> <sup>+</sup>	16 ± 17.09	9.742 ± 7.659	0.491 ± 0.147
Sodium, Na <sup>+</sup>	7 ± 1.568	8.613 ± 0.822	0.589 ± 0.016
Magnesium, Mg <sup>2+</sup>	3.286 ± 0.863	3.097 ± 0.389	1.705 ± 0.029
Potassium, K <sup>+</sup>	7.143 ± 2.068	6.677 ± 0.923	2.192 ± 0.057
Calcium, Ca <sup>2+</sup>	75.643 ± 17.72	32.355 ± 6	54.624 ± 5.58
Total OC	136.714 ± 193.347	104.14 ± 98.035	36.673 ± 13.715
Total EC	17.643 ± 31.708	15.785 ± 15.165	25.537 ± 7.833
Carbonate, CO <sub>3</sub> <sup>2-</sup>			11.751 ± 3.304
Total Carbon	409.881 ± 220.945	235.333 ± 110.398	78.44 ± 28.921
Sodium, Na			
Magnesium, Mg			
Aluminum, Al	58.238 ± 12.122	5.796 ± 3.234	18.202 ± 0.146
Silicon, Si	177.738 ± 31.421	19.538 ± 4.78	86.095 ± 0.467
Phosphorous, P			1.191 ± 0.073
Sulfur, S	4.976 ± 8.35		0.7 ± 0.074
Chlorine, Cl			0.033 ± 0.041
Potassium, K	23.143 ± 5.036	2.968 ± 1.469	12.7 ± 0.046
Calcium, Ca	121.571 ± 21.891	8.667 ± 3.714	100.154 ± 0.383
Scandium, Sc			
Titanium, Ti	3.214 ± 1.638	0.065 ± 0.704	2.009 ± 0.017
Vanadium, V	0.286 ± 0.693	0.108 ± 0.313	0.026 ± 0.006
Chromium, Cr		0.011 ± 0.286	0.017 ± 0.005
Manganese, Mn		0.237 ± 3.178	0.867 ± 0.063
Iron, Fe	40.643 ± 6.904	3.71 ± 0.644	22.505 ± 0.066
Cobalt, Co	0.143 ± 0.692	0.108 ± 0.313	
Nickel, Ni	0.286 ± 3.242	0.161 ± 1.46	0.014 ± 0.028
Copper, Cu			0.029 ± 0.068
Zinc, Zn	0.024 ± 7.848	0.333 ± 3.513	0.108 ± 0.068
Gallium, Ga			0.007 ± 0.065
Arsenic, As			0.003 ± 0.065

	<b>Unburned</b>	<b>Burnt (Ridge)</b>	<b>Burnt (Wash)</b>
Selenium, Se			
Bromine, Br	0.333 ± 1.333	0.043 ± 0.602	0.083 ± 0.012
Rubidium, Rh			0.085 ± 0.008
Strontium, Sr	0.143 ± 1.311		0.43 ± 0.012
Yttrium, Y	0.238 ± 0.905	0.065 ± 0.412	0.012 ± 0.008
Zirconium, Zr	0.048 ± 3.504	0.032 ± 1.557	0.111 ± 0.031
Niobium, Nb			
Molybdenum, Mo	0.905 ± 2.268	0.011 ± 1.045	0.003 ± 0.022
Palladium, Pd	0.762 ± 2.86	0.667 ± 1.292	
Silver, Ag	1.595 ± 3.177	0.785 ± 1.431	
Cadmium, Cd	0.5 ± 5.048	0.215 ± 2.279	
Indium, In	0.071 ± 4.023	0.409 ± 1.83	
Tin, Sn		0.172 ± 2.655	
Antimony, Sb	3.238 ± 7.685	0.774 ± 3.462	0.015 ± 0.068
Cesium, Cs			
Barium, Ba	2.095 ± 12.17	5.183 ± 5.541	
Lanthanum, La	6.857 ± 21.221		
Cerium, Ce			
Samarium, Sa			0.074 ± 0.298
Europium, Eu	5.69 ± 28.418		
Terbium, Tb		2.774 ± 13.022	0.152 ± 0.254
Hafnium, Hf			0.016 ± 0.117
Tantalum, Ta	4.881 ± 9.843	0.28 ± 4.415	
Tungsten, W			
Iridium, Ir		0.065 ± 1.311	
Gold, Au			
Mercury, Hg			
Thallium, Th	0.333 ± 1.975	0.14 ± 0.894	0.001 ± 0.014
Lead, Pb	0.143 ± 2.097		0.029 ± 0.019
Uranium, U			

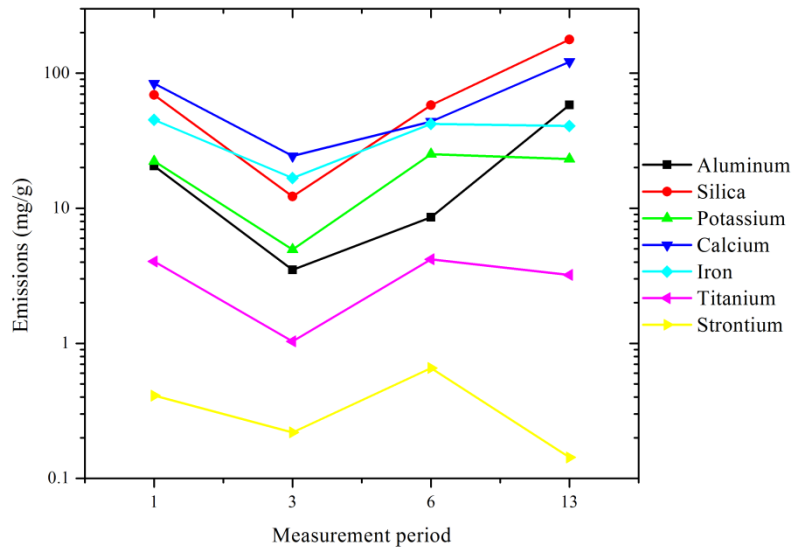


Figure A-1. Emission profiles (in  $\mu\text{g/g}$ ) of elements associated with mineral soil particles from native desert soils (Uncertainties overlap zero for: Sr for 1, 6, and 13 MAB).

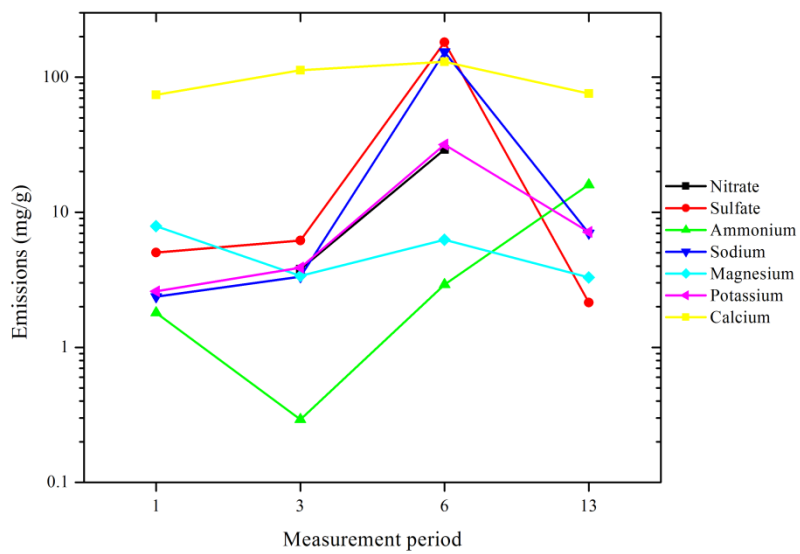


Figure A-2. Emission profiles (in  $\mu\text{g/g}$ ) of water-soluble anions and cations from native desert soils (Uncertainties overlap zero for: ammonium for 1, 3, 6, and 13 MAB; sulfate for 1 and 3 MAB).

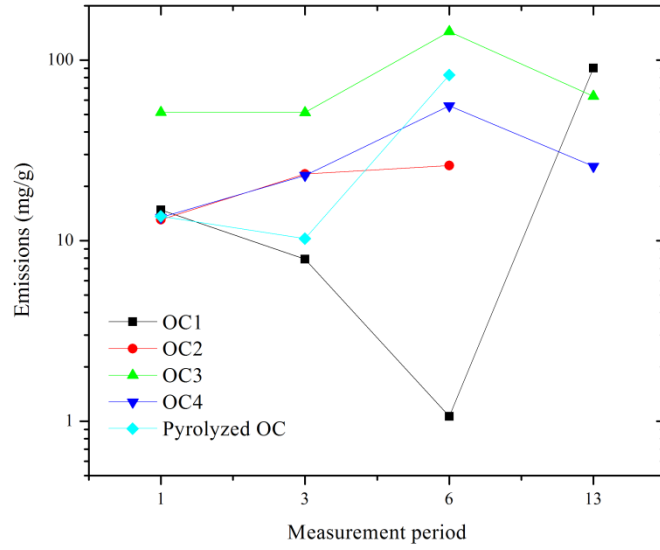


Figure A-3. Emission profiles (in  $\mu\text{g/g}$ ) of carbonaceous particles from native desert soils.

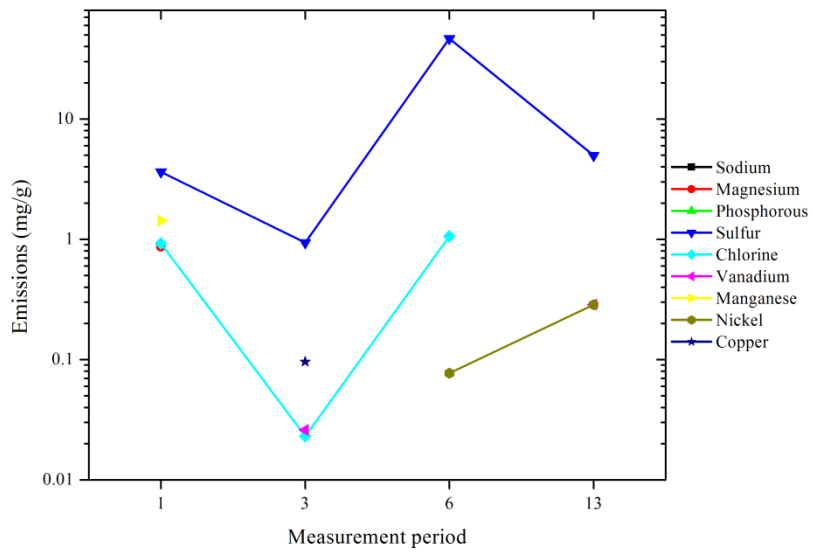


Figure A-4. Emission profiles (in  $\mu\text{g/g}$ ) of common elements from native desert soils (Uncertainties overlap zero for: Magnesium at 1 MAB; sulfur at 13 MAB, vanadium at 13 MAB; nickel at 6 and 13 MAB).

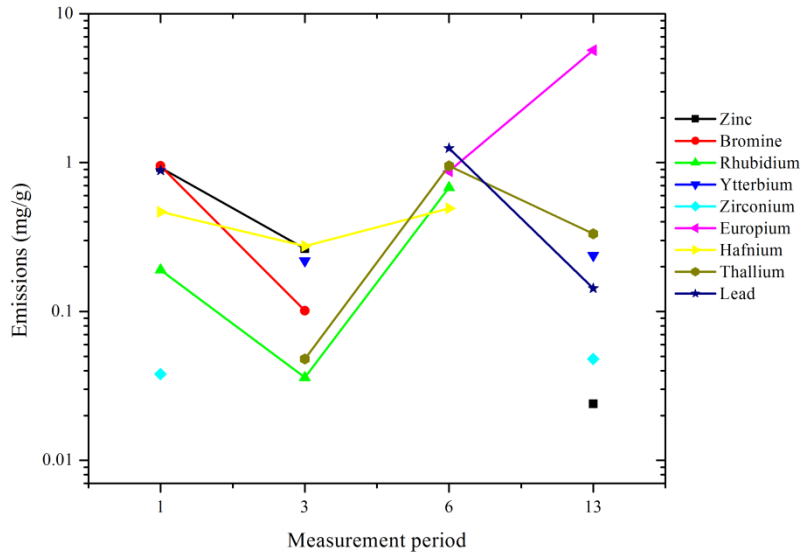


Figure A-5. Emission profiles (in  $\mu\text{g/g}$ ) of rare elements from native desert soils (Uncertainties overlap zero for: zinc at 13 MAB; ytterbium at 13 MAB; bromine at 3 and 13 MAB; rhubidium at 1 and 13 MAB; zirconium at 1 and 13 MAB; europium at 6 and 13 MAB; thallium at 6 and 13 MAB; hafnium at 1, 3, and 6 MAB).

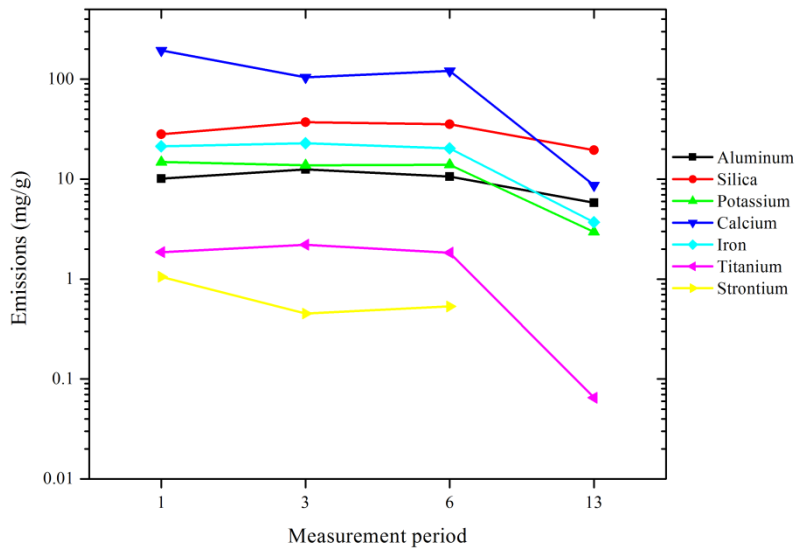


Figure A-6. Emission profiles (in  $\mu\text{g/g}$ ) of elements associated with mineral soil particles from burned ridge soils (Uncertainties overlap zero for: titanium for 13 MAB).

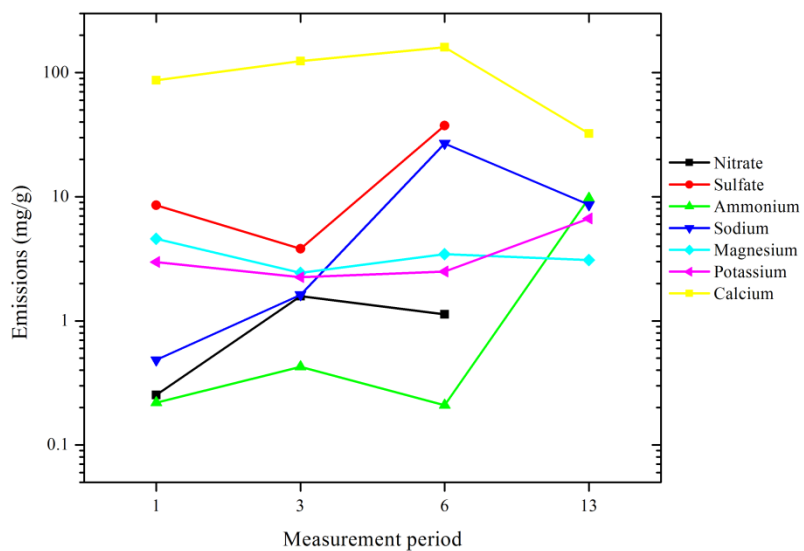


Figure A-7. Emission profiles (in  $\mu\text{g/g}$ ) of water-soluble anions and cations from burned ridge soils (Uncertainties overlap zero for: ammonium for 1, 3, and 6 MAB).

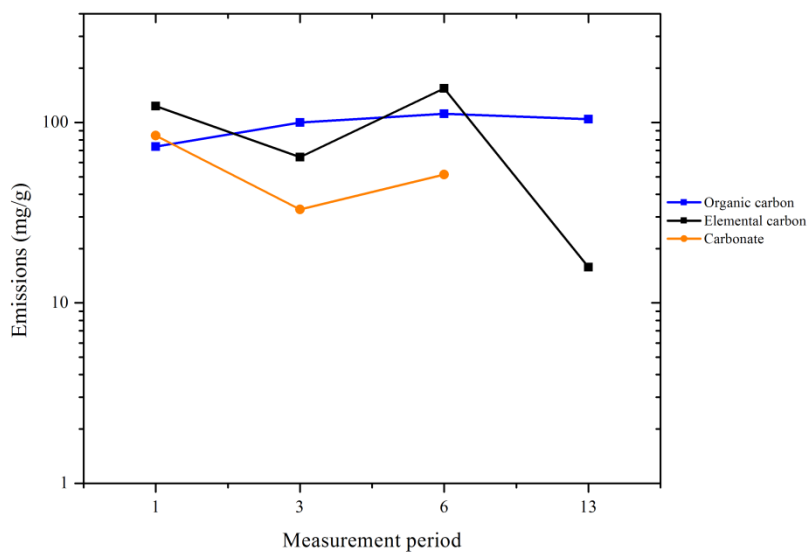


Figure A-8. Emission profiles (in  $\mu\text{g/g}$ ) of carbonaceous particles from burned ridge soils.

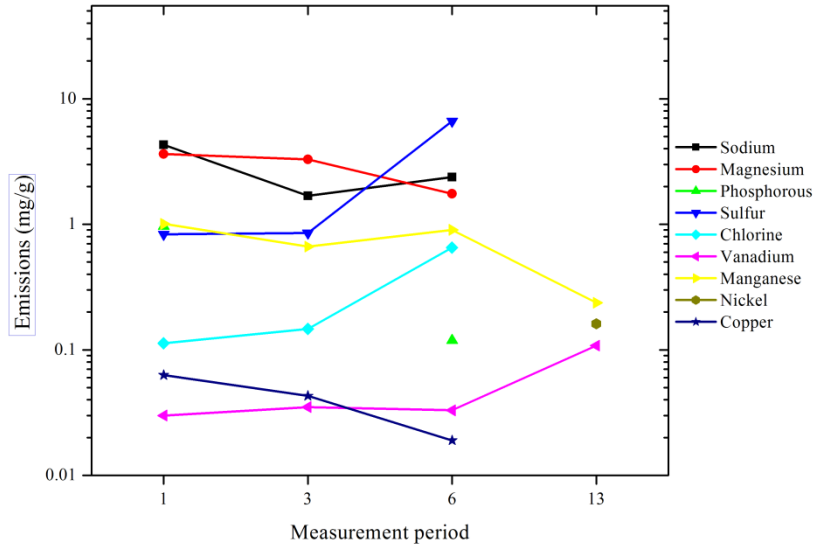


Figure A-9. Emission profiles (in  $\mu\text{g/g}$ ) of common elements from burned ridge soils (Uncertainties overlap zero for: Sodium at 3 MAB; phosphorous at 6 MAB; copper at 6 MAB; vanadium at 13 MAB; manganese at 13 MAB; nickel at 3 and 13 MAB).

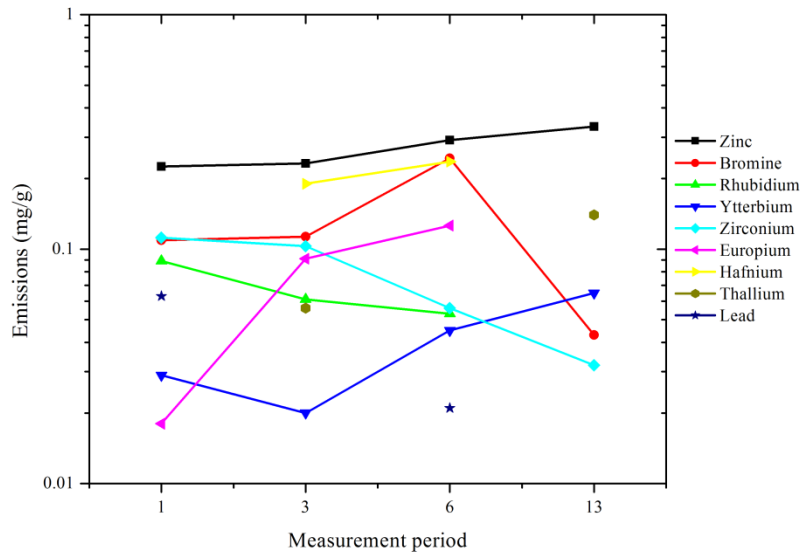


Figure A-10. Emission profiles (in  $\mu\text{g/g}$ ) of rare elements from burned ridge soils (Uncertainties overlap zero for: lead at 6 MAB; ytterbium at 3 and 13 MAB; thallium at 3 and 13 MAB; zirconium at 6 and 13 MAB; hafnium at 3 and 6 MAB; and europium at 1, 3, and 6 MAB).

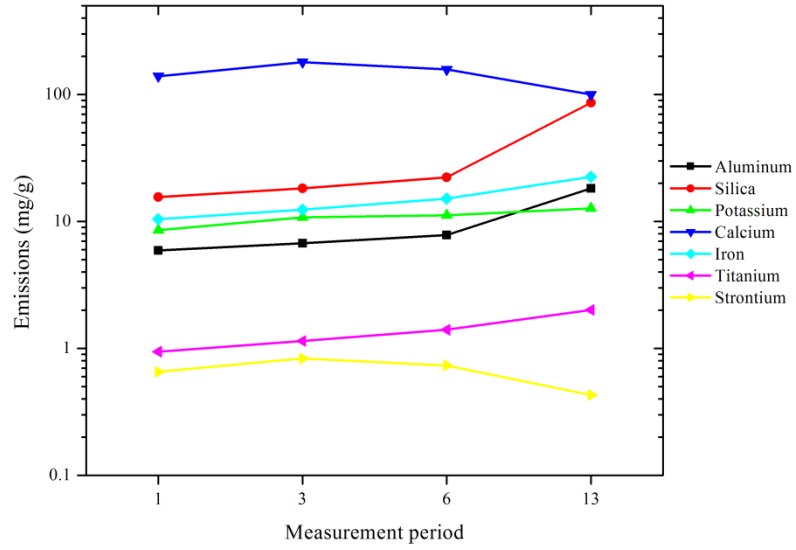


Figure A-11. Emission profiles (in  $\mu\text{g/g}$ ) of elements associated with mineral soil particles from native desert soils.

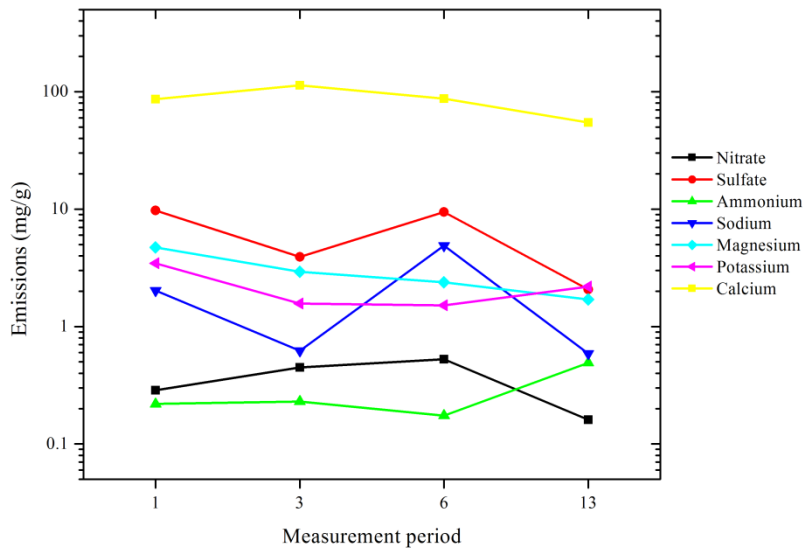


Figure A-12. Emission profiles (in  $\mu\text{g/g}$ ) of water-soluble anions and cations from native desert soils (Uncertainties overlap zero for: ammonium for 3 and 6 MAB).

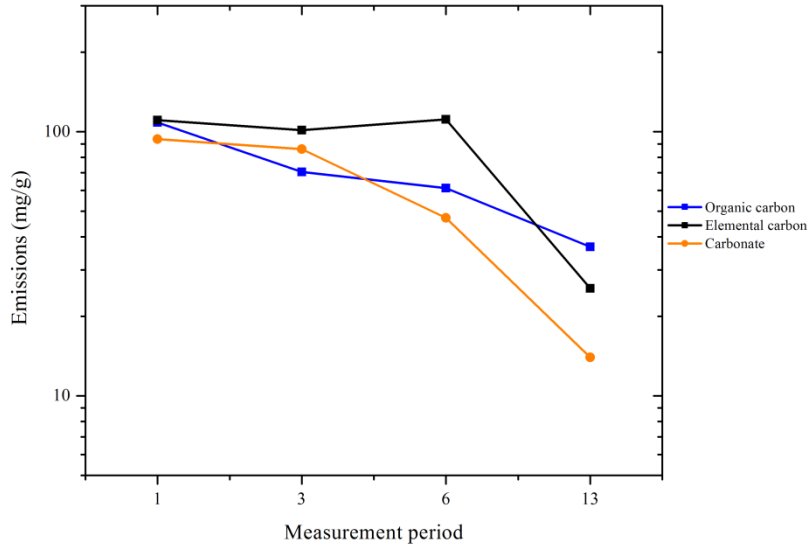


Figure A-13. Emission profiles (in  $\mu\text{g/g}$ ) of carbonaceous particles from native desert soils.

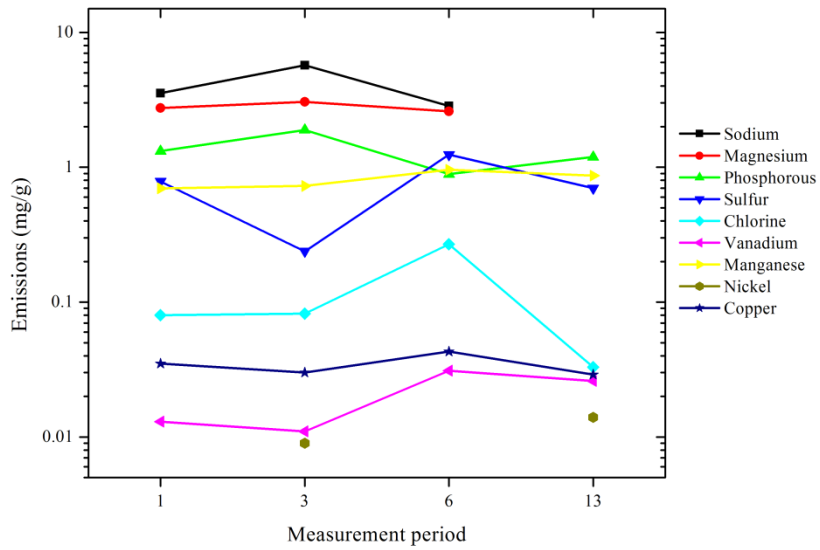


Figure A-14. Emission profiles (in  $\mu\text{g/g}$ ) of common elements from native desert soils (Uncertainties overlap zero for: chloride at 13 MAB; nickel at 13 MAB; and copper at 13 MAB).

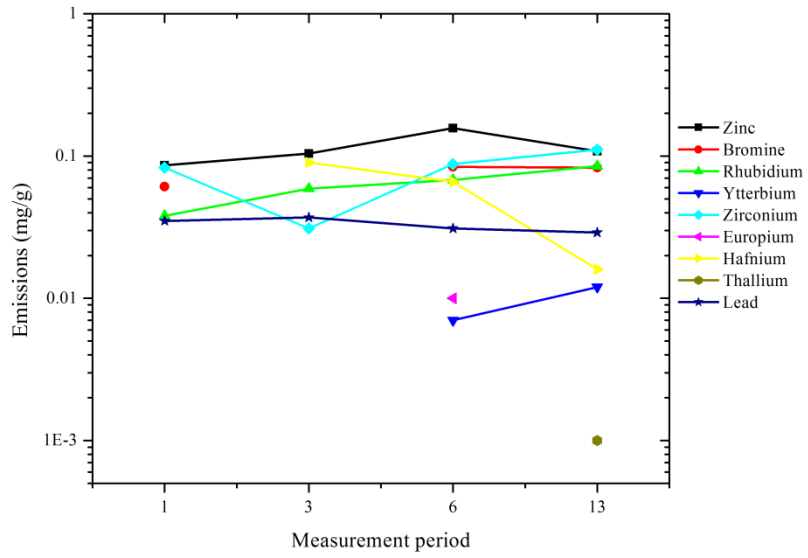


Figure A-15. Emission profiles (in  $\mu\text{g/g}$ ) of rare elements from native desert soils (Uncertainties overlap zero for: zirconium at 3 MAB; ytterbium at 6 MAB; europium at 6 MAB; thallium at 3a and 13 MAB; and hafnium at 3, 6, and 13 MAB).